Longitudinal discontinuities in riverine greenhouse gas dynamics generated by dams and urban wastewater

Hyojin Jin[1], Tae Kyung Yoon[2], Most Shirina Begum[1], Eun-Ju Lee[3], Neung-Hwan Oh[3], Namgoo Kang[4, 5], Ji-Hyung Park[1]

[1]Department of Environmental Science and Engineering, Ewha Womans University, Seoul 03760, Republic of Korea
[2]Division of Environmental Strategy, Korea Environment Institute, Sejong 30147, Republic of Korea
[3]Graduate School of Environmental Studies, Seoul National University, Seoul 08826, Republic of Korea
[4]Center for Gas Analysis, Korea Research Institute of Standards and Science, Daejeon 34113, Republic of Korea
[5]Science of Measurement, University of Science and Technology, Daejeon 34113, Republic of Korea

Correspondence to: Ji-Hyung Park (jhp@ewha.ac.kr); Namgoo Kang (nkang@kriss.re.kr)

Abstract.

Riverine emissions of CO_2 and other greenhouse gases (GHGs) represent crucial, but poorly constrained components of the global GHG budgets. Three major GHGs – CO_2, CH_4, and N_2O – have rarely been measured simultaneously in river systems modified by human activities, adding uncertainties to the estimates of global riverine GHG emissions. Measurements of C isotopes in dissolved organic carbon (DOC), CO_2, and CH_4 were combined with basin-wide surveys of three GHGs in the Han River, South Korea to investigate dams and urban water pollution as major controls on GHG dynamics in the highly human-impacted river basin with a population >25 million. Monthly monitoring and two-season comparison were conducted at 6 and 15 sites, respectively, to measure surface water concentrations of three GHGs, along with DOC and its optical properties. The basin-wide surveys were complemented with a boat cruise along the lower reach and synoptic samplings along a polluted tributary delivering effluents from a large wastewater treatment plant (WWTP) to the lower reach. The basin-wide surveys of three GHGs revealed distinct increases in the concentrations of three gases along the lower reach receiving urban tributaries enriched in GHGs and DOC. Compared to the spatial patterns of GHGs observed in the upper and lower reaches, the levels of pCO$_2$ were consistently lower across the impounded middle reach, whereas concentrations of CH_4 and N_2O were relatively high in some impoundment-affected sites. Similar levels and temporal variations in three GHGs at the WWTP effluents and the receiving tributary indicated a disproportionate contribution of the WWTP to the tributary exports of DOC and GHGs. Measurements of $\delta^{13}C$ in surface water CO_2 and CH_4 sampled during the cruise along the lower reach, combined with $\delta^{13}C$ and $\Delta^{14}C$ in dissolved organic matter (DOM) sampled across the basin, implied that longitudinal decreases in $\Delta^{14}C$ in DOM might be associated with wastewater-derived, old DOM in urban tributaries, which, together with enhanced photosynthesis and CH_4 oxidation in the eutrophic lower reach, appear to constrain downstream changes in $\delta^{13}C$ in CO_2 and CH_4. The overall results suggest that dams and urban wastewater may create longitudinal discontinuities in riverine metabolic processes leading to large spatial variations in three GHGs. Further research is required to evaluate the relative contributions of anthropogenic

and autochthonous sources to GHG pulses along the lower reach and constrain key factors for the contrasting impoundment effects including autotrophy-driven decreases in pCO_2 and in-lake production of CH_4 and N_2O.

1 Introduction

35   A growing body of research on greenhouse gas (GHG) emissions from inland waters has recently generated various global syntheses of CO_2 and CH_4 data (Cole et al., 2007; Bastviken et al., 2011; Raymond et al., 2013; Lauerwald et al., 2015; Stanley et al., 2016; Marx et al., 2017) and conceptual frameworks incorporating anthropogenic perturbations as a critical driver of riverine biogeochemical processes in human-impacted river systems (Kaushal et al., 2012; Regnier et al., 2013; Park et al., 2018). Recent studies in large river systems such as the Amazon and Congo have identified wetlands as previously

40   unrecognized sources of CO_2 and organic matter (Abril et al., 2014; Borges et al., 2015). However, these recent efforts have been hampered by data scarcity and inequality and inadequate consideration of multiple GHGs co-regulated by a wide range of concurrent environmental changes including anthropogenic perturbations. While pCO_2 calculated from available water quality data such as pH and alkalinity has been used widely to estimate CO_2 emissions from a wide range of inland water systems (Lauerwald et al., 2013; Raymond et al., 2013), substantial overestimation of pCO_2 can occur in acidic, organic-rich

45   inland waters due to the contribution of organic acids to alkalinity and the limited carbonate buffering (Abril et al., 2014). Another critical issue is the lack of reliable measurements of the surface water partial pressure of CO_2 (pCO_2) in many of large river systems across Asia and Africa (Raymond et al., 2013; Lauerwald et al., 2015). Furthermore, three major GHGs (CO_2, CH_4, and N_2O) have rarely been measured simultaneously across different components of river systems except for a small number of large, 'natural' rivers such as the Amazon (Richey et al., 1988) and the Congo (Borges et al., 2015; Teodoru et al.,

50   2015) or highly human-impacted systems (Smith et al., 2017; Wang et al., 2017b; Borges et al., 2018). While global river systems are now subject to multiple environmental stresses, including those caused by human-made structures and climate change, most research efforts have been focused on one or a few components of the concurrent perturbations. A more integrative approach addressing multiple GHGs and anthropogenic perturbations is required to better constrain the controlling factors and mechanisms for GHG emissions from increasingly human-impacted river systems worldwide.

55   A small number of studies that measured CO_2, CH_4, and N_2O together in large rivers such as the Amazon and Congo have revealed some common longitudinal patterns of three GHGs driven by interrelated sources and production mechanisms (Richey et al., 1988; Borges et al., 2015). For instance, Richey et al. (1988) found large increases in dissolved CO_2 and CH_4 and slight reductions in N_2O in the Amazon mainstem downstream of large floodplains. They suggested that predominant anaerobic metabolism might drive the enhanced release of CO_2 and CH_4 from floodplains, concurrently consuming N_2O

60   through more efficient denitrification under oxygen-depleted conditions. A regional-scale comparison of three GHGs in 12 African rivers also showed similar relationships between three GHGs and wetland extents within the basin (Borges et al., 2015). These previous studies have used positive relationships between dissolved organic carbon (DOC) concentrations and CO_2 and other GHGs as an indication of the riverine heterotrophy driving in-stream production of GHGs (Borges and Abril,

2011; Borges et al., 2015; Teodoru et al., 2015). The widely used concept of river continuum from headwater to mouth assumes
gradual and continual changes in riverine organic matter composition and metabolic processes corresponding to downstream
variations in environmental conditions and biotic communities along the river (Vannote et al., 1980). However, it remains
unexplored whether the traditional view of gradual longitudinal variations in riverine organic matter composition and its
transformations can explain riverine dynamics of GHGs driven by a combination of multiple environmental factors specific to
various natural and human-impacted river systems.

Measurements of multiple GHGs in highly human-impacted river systems have provided drastically different pictures of the
longitudinal and seasonal patterns of GHGs from those observed in large natural rivers (Silvennoinen et al., 2008; Burgos et
al., 2015; Crawford et al., 2016; Smith et al., 2017; Wang et al., 2017b). A growing number of dams constructed on rivers
worldwide have altered riverine flows of water and materials to the oceans, trapping over 100 billion metric tons of sediment
and up to 3 billion metric tons of C in the reservoirs constructed over the last five decades (Syvitski et al., 2005). The trapping
of sediments and nutrients in reservoir sediments, combined with increased water retention time and improved light conditions
promoting primary production, can alter significantly the rate of production and consumption of CO_2 and CH_4 in impounded
waters (Maavara et al., 2017). Many studies have examined impoundment effects on GHG emissions from various types and
sizes of dams including hydroelectric dams, often reporting contrasting results such as large pulse emissions of CO_2 and CH_4
from the flooded vegetation and sediments following dam construction and an enhanced primary production and CO_2 sink in
eutrophic reservoirs (Abril et al., 2005; Chen et al., 2009; Barros et al., 2011; Hu and Cheng, 2013; Maeck et al., 2013;
Crawford et al., 2016; Maavara et al., 2017; Shi et al., 2017). These contrasting impoundment effects can be explained by the
shifting balance between autotrophy and heterotrophy at diel to decadal timescales (Park et al., 2018). However, little is known
about complex interplays among multiple factors and mechanisms concurrently affecting the production and consumption of
three GHGs. While enhanced primary production and anaerobic metabolism may play a determining role in long-term changes
in CO_2 and CH_4 emissions from the water column and sediments in impounded reaches, external inputs of organic matter and
nutrients have also been suggested as a primary control on GHG emissions from urban streams and rivers (Alshboul et al.,
2016; Smith et al., 2017; Wang et al., 2017b). Longitudinal surveys conducted along urbanized rivers have observed large
pulsatile increases in CO_2 and other GHGs in rivers receiving the effluents from wastewater treatment plants (WWTPs)
(Garnier et al., 2013; Burgos et al., 2015; Alshboul et al., 2016; Yoon et al., 2017). WWTP effluents and other anthropogenic
sources can not only exert direct effects on riverine GHG dynamics via discharged loads of GHGs, DOC, and nutrients but
also modify riverine metabolic regimes (Garnier and Billen, 2007; Park et al., 2018). The complexity of involved metabolic
processes, together with the multiplicity of environmental conditions and anthropogenic perturbations, poses a great challenge
for a systematic understanding of GHG dynamics in human-impacted river systems.

The Han River basin exhibits unique longitudinal variations in dominant land use and anthropogenic perturbations, offering a
venue for various biogeochemical studies of riverine organic matter and CO_2 dynamics (Fig. 1; Jung et al., 2012; Jin et al.,
2016; Yoon et al., 2017). Although headwater streams feeding into the upper reach drain largely forested mountainous terrain,
the recent expansion of croplands on steep slopes has resulted in high levels of nutrients and suspended sediment in downstream

waters receiving agricultural runoff, particularly during heavy monsoon rainfalls (Park et al., 2010). A series of dams on the middle reach of the North Han River may create "serial discontinuity" in riverine metabolic processes and GHG emissions (Ward and Stanford, 1983; Park et al., 2018), while urban tributaries draining the densely populated Seoul metropolitan area with a population >25 million discharge pulsatile loads of nutrients, DOC, and GHGs to the lower Han River (Yoon et al., 2017). Building on our previous studies focused on CO_2 dynamics along the Han River (Yoon et al., 2016, 2017), this study aims to compare basin-wide patterns of surface water CO_2, CH_4, and N_2O. The primary objective was to examine the effects of dams and urban wastewater on the spatiotemporal variations in three major GHG concentrations. Another important goal was to track longitudinal variations in major sources of DOM and GHGs by combining measurements of C isotopes in DOC, CO_2, and CH_4 with a basin-scale monitoring of three GHGs. Unlike other studies focused on the quantitative importance of inland waters as sources of GHGs, this study aims to examine basin-scale patterns of riverine GHG dynamics against the conceptual frameworks that can explain longitudinal variations in riverine dissolved organic matter (DOM) and GHGs (refer to Park et al., 2018 and references therein), so only concentration data are presented without providing estimated emissions of three GHGs. We expected that the comparison of reach-specific spatial patterns of three GHGs and C isotopic composition in DOM, CO_2, and CH_4 in the river system modified by river impoundment and pollution would provide invaluable field data essential for examining emerging concepts of anthropogenically created discontinuities in riverine metabolic processes and GHG emissions.

2 Materials and methods

2.1 Study site

The Han River (494 km), consisting of the North Han and South Han branches and the lower Han River (often called "Han River"), drains an area of 35,770 km² in the middle of the Korean Peninsula (Fig. 1; Seoul Metropolitan Government, 2017). The mean annual precipitation in the Han River basin was 1323 mm for the period from 1983 to 2014, with up to 70% of the annual precipitation concentrated during four months from June to September. Major land uses in the basin include forests (73.6%), croplands (14.1%), urban and industrial areas (2.6%), and other uses (9.7%) (Fig. S1). The highly urbanized metropolitan area along the lower reach has a large impermeable surface regarded as urban land use, accounting for 58% of the total city area of Seoul (Seoul Metropolitan Government, 2017). Sampling sites were established along a North Han River section and the lower Han River, covering forested headwater (HR1) and agricultu ral streams along the upper reach through the middle and lower reaches impounded by dams and submerged weirs to the estuary.

Along the monitored reaches of the North Han River, four large multi-purpose hydroelectric dams have been constructed since 1943. The most upstream dam (Soyang; HR5) constructed in 1973 is the largest (height: 123 m; reservoir surface area: 70 km²). The most downstream dam constructed in 1973 (Paldang; HR10) located at the confluence of the North and South Han branches regulates river flow to the lower reach and supplies 2.6 million metric tons of water per day to the 25 million metropolitan population. Three major urban tributaries [Joongnang River (JN; HR12), Tan River (TC), and Anyang River

130 (AY)] feed into the channelized lower Han River with submerged weirs at both ends. The tributary JN drains an area of 300 km^2 inhabited by 3.6 million, ~45% of which urban land use accounted for in 2014 (Seoul Metropolitan Government, 2017). Three WWTPs release treated sewage at the rate of 1.5 million m^3 d^{-1} to the tributary (JN), with the bulk (1.3 million m^3 d^{-1}) discharged from the monitored WWTP near the mouth of JN, which employs tertiary treatments including modified Ludzack Ettinger (MLE) and anaerobic-anoxic/oxic process (A_2O) (Ministry of Environment, 2015). Four WWTPs located within Seoul

135 release effluents from tertiary treatments at the rate of 4.3 million m^3 d^{-1}.

2.2 Sampling and field measurements

Basin-wide surveys were carried out at 15 sites encompassing major land uses and human-induced perturbations in the Han River basin during a summer monsoon period (July 2014) and in a dry period (May 2015) (Table 1; Figs. 1, S1). Compared to the upper reach (HR1 – HR4) located in a heavily forested watershed with some scattered agricultural areas (Fig. S1), the

140 impounded middle reach (HR5 – HR11) and the lower reach receiving heavy loads of urban sewage (HR12 – HR15) are subject to stronger anthropogenic perturbations. At 6 selected sites (HR1, HR2, HR4, HR8, HR11, and HR14), routine monitoring was continued at monthly intervals from July 2014 to July 2015, except for two winter months (January and February 2015). In addition to two-season surveys, 13 samplings were conducted at an outlet of the tributary JN (HR12) from May 2015 to December 2017. In November 2015 and May 2016, additional samples were collected at 8 locations from a

145 forested headwater stream to the outlet along the JN (Fig. 1; Fig. S1). The 8 sites were selected to cover the spatial pattern of land use, ranging from the forested upper reach to the increasingly urbanized downstream reaches (Fig. S1). The tributary samplings were complemented with 4 samplings at a discharge from a WWTP located a few km upstream of the JN outlet. To explore spatially resolved patterns of riverine concentrations of three GHGs along the lower Han River, water and gas samples were collected at 8 locations during a boat expedition on 10 June 2016 that also aimed at continuous underway measurements

150 of pCO_2 using automated pCO_2 measurement systems as reported by Yoon et al. (2017).

In each sampling, water samples were collected from a depth of 10–20 cm below the water surface in the middle of the stream channel or > 2 m away from the river bank. Spot water samples for chemical analysis were collected through a peristaltic pump (Masterflex E/S portable sampler, Cole-Palmer Instrument Co., USA) into acid-washed amber glass bottles. At the same sampling point we measured water temperature, pH, electrical conductivity (EC), and dissolved oxygen (DO) using a portable

155 pH meter (Orion 5-Star Portable, Thermo Scientific, USA). Surface water concentrations of three GHGs were measured by a manual headspace equilibration method (Kling et al., 1992; Yoon et al., 2016). Headspace equilibration was performed using a polypropylene syringe (60 ml; HSW Norm-Ject Luer Lock Tip; Henke-Sass Wolf GmbH, Germany) to collect a 30 mL water sample and then a 30 mL ambient air sample. Another air sample was collected to measure gas concentrations in the ambient air. The syringe containing the water and air samples was shaken vigorously for 2 min; then ~20 mL of the equilibrated air

160 was stored in a pre-evacuated 12 mL glass vial (Exetainer, Labco, UK). The stored gas sample volume was larger than the vial volume to create overpressure and hence minimize gas concentration change associated with potential gas leakage. Vials had been flushed with high-purity N_2 gas before the filled N_2 gas was evacuated by a pump. Gas analysis was performed usually

within three days after the sampling. Air temperature and barometric pressure were measured in situ by a portable sensor (Watchdog 1650 Micro Station, Spectrum Technologies Inc., USA). Barometric pressure, together with water temperature, was used to calculate concentrations of three GHGs from the gas concentrations of the equilibrated air and ambient air samples based on Henry's law (Hudson, 2004). Details on the calculation algorithms and Henry's law constants for three GHGs are provided in Hudson (2004).

2.3 Laboratory analyses

The equilibrated headspace air sample, as well as a sample from the ambient air used for equilibration, was injected into a GC (7890A, Agilent, USA) equipped with an FID coupled with a methanizer (for analysis of CH_4 and CO_2), a μECD (for N_2O analysis), and a Supelco Hayesep Q 12 ft 1/8" column for the simultaneous measurement of three GHGs. High-purity N_2 gas (99.999%) was used as carrier gas at a constant flow rate of 25 mL min^{-1}. The flow rate of the reference gas was 5 mL min^{-1} for FID (N_2) and 2 mL min^{-1} for μECD (Ar/CH_4).Temperature settings include the inlet at 250°C, the oven at 60°C, the valve box at 100°C, FID at 250°C, and μECD at 300°C. The volume of the sample loop was 1 mL. Standard reference gases of three GHGs in N_2 balance (RIGAS Corporation, Korea) were used to calibrate the GC signals. The gas concentrations in these calibration standards were verified in the gas analysis laboratory of Korea Research Institute of Standards and Science (KRISS) that established the national measurement standards of gravimetrically prepared CO_2 in dry air and certified by a suite of gas analysis (Min et al., 2009). Additional headspace equilibration samples collected during the boat cruise in June 2016 were analysed for stable C isotope ratios of CO_2 ($\delta^{13}C_{CO2}$) and CH_4 ($\delta^{13}C_{CH4}$) by a GasBench-IRMS (ThermoScientific, Bremen, Germany) at the UC Davis Stable Isotope Facility.

Water samples were filtered through pre-combusted (450°C) glass fiber filters (GF/F, Whatman; nominal pore size 0.7 μm) at the laboratory. The concentration of total suspended solid (TSS) was measured as the difference in the filter weight before and after drying at 60°C for 48 hours. Filtered water samples were analyzed for dissolved organic C, fluorescence excitation-emission matrices (EEMs), UV absorbance, total alkalinity (TA), dissolved ions, and chlorophyll a (Chl a). For quality control of all chemical analyses, standards with known concentrations and ultrapure water were analyzed for every batch of ten samples and triplicate analysis was performed for approximately 10% of all analyzed samples to assess instrumental stability and accuracy.

DOC was measured by a total organic carbon (TOC) analyzer using high-temperature combustion of OM followed by thermal detection of CO_2 (TOC-V_{CPH}, Shimadzu, Japan). UV absorbance was measured across the wavelength range from 200 to 1100 nm using a UV-Vis spectrophotometer (8453, Agilent, USA). Fluorescence EEMs were collected on a fluorescence spectrophotometer (F7000, Hitachi, Japan) by simultaneous scanning over excitation wavelengths from 200 to 400 nm at 5 nm interval and emission wavelengths from 290 to 540 nm at 1 nm interval. Scan speed was 2400 nm min^{-1} and the bandwidth was set to 5 nm for both excitation and emission. UV absorbance and fluorescence data were used to calculate specific UV absorbance at 254 nm ($SUVA_{254}$) (Weishaar et al., 2003), fluorescence index (FI) (McKnight et al., 2001), humification index

195 (HI) (Zsolnay et al., 1999), and common fluorescence EEM components (Fellman et al. 2010). Three fluorescent EEM components termed C1 (excitation/emission peaks at 325/467 nm), C2 (315/404 nm), and C3 (275/354 nm) were used to represent humic-like, microbial humic-like, and protein-like fluorescence, respectively (Fellman et al., 2010). TA was determined with 40–80 mL filtered samples on an automated electric titrator (EasyPlus Titrator Easy pH, Metrohm, Switzerland) based on the Gran titration method (Gran, 1952). Strong acid (0.1 N HCl) was used to titrate well beyond the

200 equivalence point at pH between 4 and 3. Ions dissolved in water samples were analysed on an ion chromatograph (883 Basic IC plus, Metrohm, Switzerland). Chl a was analyzed spectrophotometrically following filtration on GF/C filters and acetone extraction (American Public Health Association, 2005).

Dual carbon isotopes analyses were conducted for water samples collected from six monthly monitoring sites and the JN WWTP effluents. Subsamples of filtered water samples were kept frozen before analysis. For Δ^{14}C-DOC analysis, each water

205 sample was acidified by 40% H_3PO_4 solution and sparged by helium gas to remove inorganic carbon. Then, the sample was oxidized with ultrahigh purity oxygen gas using UV lamp for 4 hours (Raymond and Bauer, 2001). The oxidized CO_2 was separated cryogenically with liquid N_2 in a vacuum line and sealed in a pre-baked pyrex tube. The CO_2 samples in the sealed pyrex tubes were sent to the National Ocean Sciences Accelerator Mass Spectrometry (NOSAMS) facility at the Woods Hole Oceanographic Institution for dual isotope analysis (Δ^{14}C and δ^{13}C) where accelerated mass spectrometer and isotope ratio

210 mass spectrometer were used for Δ^{14}C and δ^{13}C analysis, respectively (http://www.whoi.edu/nosams/home). The CO_2 samples were transformed to graphite targets for Δ^{14}C analysis by accelerated mass spectrometry.

2.4 Statistical analysis

Most dissolved GHGs and water quality data were not normally distributed, and their distribution patterns varied with river reach and measured parameter. Therefore, Kendall rank correlation, as a non-parametric test, was performed using the Kendall

215 package of R (R Development Core Team, 2018) to investigate the relationships between water quality variables and dissolved GHGs both for the whole Han River basin and for each of the upper, middle, and lower reaches. For the monthly monitoring data, seasonal differences in three GHGs were analysed by the non-parametric Kruskal-Wallis analysis of variance followed by Dunn's multiple comparisons. For reach-specific analysis, sampling sites were grouped into three reaches, as shown on Fig. 1. The upper reach includes sites HR1 to HR4 (outlet of the major tributary to the Lake Soyang, HR5). The middle reach

220 covers the first dam on the monitored transect (HR5) through three downstream dams and ends up at HR 11,which receives discharge from the most downstream dam (HR10). The lower reach includes the mainstem (HR13, HR14, and HR15) and tributary sites [TC, JN (HR12), and AY] downstream of the first submerged weir in Seoul (Fig. 1). Relationships between three GHGs and water quality measurements were examined by regression analysis conducted with the data pooled for the whole basin and each cluster of three reaches and urban tributaries. Spatial variations among three reaches were further

225 examined by principal component analysis (PCA).

3. Results

3.1 Longitudinal variations in GHG concentrations and DOM characteristics along the Han River

Two basin-wide surveys from the forested headwater stream (HR1) through the impounded middle reach to the highly urbanized lower reach, combined with the monthly monitoring at six selected sites, revealed distinct longitudinal patterns of pCO_2 and concentrations of CH_4 and N_2O along the Han River (Figs. 2, 3, 4; Tables 1, S1, S2, S3). The concentrations of three GHGs were relatively low along the upper reach, although small, but noticeable increases occurred in the agricultural stream (HR2) compared to the generally low values found in the forested headwater stream (HR1) (Fig. 2; Table 1). Levels of pCO_2 in the middle reach (HR5 – HR11; 51 – 761 µatm) tended be lowest when compared with upper and lower reaches and were particularly low at sites within a few km upstream or downstream of the cascade dams. In contrast, N_2O and CH_4 concentrations were higher at one (HR6; 212 nM N_2O L^{-1}) or three dam sites (HR6, HR7, and HR10; 693 – 748 nM CH_4 L^{-1}), respectively, compared to the upstream or downstream reaches of the dam sites (Table 1). For all three GHGs, large downstream increases were found along the lower reach flanked by two submerged weirs (HR12 – HR14). Gas concentrations at some lower-reach sites approached or exceeded the levels found in three tributaries draining the urban sub-catchments located in Seoul and surrounding suburban areas (Fig. 2). pCO_2 tended to be higher in summer than in other seasons at all monthly monitoring sites except HR8 and HR 11, which are subject to direct or indirect influences of the cascade dams along the middle reach. There was no clear seasonality in CH_4 and N_2O across the sites, but at the lower-reach site HR14 the concentrations of two gases tended to be higher in spring and summer than in fall and winter (Fig. S2).

DOC concentrations and FI exhibited overall downstream increases along the mainstem toward the river mouth with the exception of relatively high FI values in the agricultural stream (Fig. 3; Tables S1, S2, S3). When Mann-Whitney U tests were conducted to detect downstream changes between two successive sites, both DOC and FI were significantly different between two mainstem sites (HR11, HR14) and the urban tributary JN (HR 12). HIX generally decreased downstream along the river, with significant changes occurring during transitions from HR1 to HR2 and from HR4 to HR8 (Fig. 3). The concentrations of three measured nutrients (NH_4^+, NO_3^-, and PO_4^{3-}) were generally higher at the agricultural stream (HR2) and the lower-reach sites (HR12 and HR14) than at the other sites (Fig. 3; Tables S1, S2, S3). The comparison of monthly water quality measurements between the six sites and the urban tributary (HR12), together with the proportion of tributary discharge in the mainstem flow ranging from ~5% in the monsoon period to 12% in dry seasons, points to the disproportionate influence of urban tributary inputs on the downstream increases in concentrations of DOC and nutrients observed in the lower reach (Fig. 3). The urban tributary was highly enriched in DOC, FI, protein-like DOM moieties (C3/DOC), and three nutrients, whereas it exhibited relatively low values of pH, DO, HIX, and Chl a (Fig. 3; Tables S1, S2, S3). Downstream changes in all water quality measurements from HR11 to HR14 along the lower reach appeared to correspond to either very high or very low values observed in the tributary (HR12) compared to the upstream values.

When all measurements were pooled for the whole river basin, at least one of three GHGs exhibited an overall negative relationship with pH (pCO_2) and DO (pCO_2 and CH_4) and a positive relationship with DOC (all three GHGs) (Fig. 4).

Regression analysis conducted for each group of three reaches and urban tributaries identified several significantly negative or positive relationships that generally conformed to the overall trends shown for the whole basin (Fig. 4). A positive relationship between DO and N_2O established in the lower reach was noticeable given no significant relationship found for the other reaches. Reach-specific clustering of data was also found on a PCA scatter plot with two primary components accounting for 60.3% of the total data variation (Fig. S3). Whereas the middle-reach data exhibited considerable overlaps with portions of the larger scatters displayed by the upper and lower reaches, the majority of the tributary data were distinct from this overlap.

Kendall rank correlation analyses conducted with all measurements grouped for each of three reaches revealed reach-specific patterns of significant correlations for three GHGs (Fig. 5; Table S4). Significant negative correlations were found between pCO_2 and three related water quality measurements – pH, DO, and Chl a in the lower reach. These negative correlations were either absent for N_2O or significant only with DO in the case of CH_4. Compared to no or weak correlations observed for the upper and middle reaches, some parameters measured in the lower reach, including water temperature, PO_4^{3-}, C1/DOC, and C2/DOC, exhibited strong positive correlations with pCO_2. Values of pCO_2 measured at the middle reach sites had some negative correlations with pH, TA, water temperature, cations (Na^+, K^+, and Mg^{2+}), and anions (Cl^- and SO_4^{2-}). These shifting correlations across the reaches were also found for CH_4 and N_2O, but to varying degrees. CH_4 in the lower reach had significant, but relatively weak correlations with PO_4^{3-}, C1/DOC, and C2/DOC, whereas N_2O showed strong positive correlations with parameters such as EC, TA, all measured cations, Cl^-, NO_3^-, SO_4^{2-}, DOC, FI, and C3/DOC. In the case of CH_4, stronger correlations were found in the upper reach, including pH, EC, TA, cations (K^+, Ca^{2+}, and Mg^{2+}), anions (Cl^- and SO_4^{2-}), FI, and C3/DOC, but these correlations were weaker or insignificant in the middle or lower reach.

3.2 Longitudinal variations in GHG concentrations and DOM characteristics along an urban tributary

Two synoptic samplings along the urban tributary (JN), complemented with additional samplings at a tributary outlet (HR12) and an upstream WWTP discharge, pointed to WWTP effluents driving the concentrations of three GHGs, DOC, and nutrients measured at the tributary outlet (Fig. 6; Table S5). Similar ranges of three GHG concentrations observed in the WWTP effluents and the tributary outlet corroborate the dominant contribution of WWTP effluents to the tributary GHG exports to the lower Han River. Both pCO_2 and N_2O concentrations increased abruptly along the most downstream reach after passing the WWTP located within a few km upstream. In contrast, CH_4 concentrations exhibited relatively large fluctuations along the middle reach, ending up at the intermediate levels observed for the upper to middle reaches in the WWTP effluents and the tributary outlet. Corresponding to the large scatter of the box plots representing three GHG concentrations measured at the WWTP effluents and outlet site, two locations exhibited similar patterns of temporal variations in GHG concentrations. The observed temporal variations in gas concentrations were not significantly related to fluctuations in temperature, precipitation, and streamflow measured near the tributary outlet site, although three gases exhibited some decreases in concentration during wet summer months in 2016 and 2017 (Fig. 6d).

3.3 C isotopes in DOM, CO_2, and CH_4

Dual C isotope analyses of DOM samples collected at seven sites provided information on the longitudinal evolution of the stable and radioactive C isotope ratios along the Han River (Fig. 7; Table S6). In both wet-season (July 2014) and dry-season (May 2015) samplings, $\Delta^{14}C$ generally decreased downstream toward the river mouth, with higher values observed during the July sampling across the mainstem sites. An exceptionally high value was found at the second most downstream mainstem site (HR11), which is located 17 km downstream of the last of the cascade dams. The values of $\Delta^{14}C$ measured in the urban tributary and WWTP effluent (around −100) were below those measured for all mainstem sites. $\delta^{13}C$ was highly variable at two middle-reach sites and increased almost linearly from the second most downstream site through the urban tributary and WWTP effluents to the last site (Fig. 7).

Concentrations of three GHGs (Fig. 8; Table S7) combined with $\delta^{13}C$ in CO_2 and CH_4 (Fig. 8; Table S8) collected along the lower Han River during a cruise expedition revealed clear tributary effects on the C isotopic composition of two GHGs sampled at the mainstem sites. $\delta^{13}C_{CO2}$ values ranging from −20.9 to −16.7‰ were distinctively higher than the range of $\delta^{13}C_{DOC}$ measured at the same sites (−28.2 to −20.6‰). $\delta^{13}CO_2$ continued to increase toward the river mouth, with its values bracketed by those measured for the two upstream tributaries and a downstream tributary. The downstream tributary had lower pCO_2, higher $\delta^{13}CO_2$, and higher concentrations of CH_4 and Chl a relative to the upstream tributaries. The values of $\delta^{13}CH_4$ also showed an overall increasing trend along the lower reach, except for some localized decreases downstream of the urban tributary (HR12).

4 Discussion

4.1 Reach-specific patterns and controls on three GHGs

Building on our previous report on CO_2 dynamics in the Han River basin (Yoon et al., 2016, 2017), this study provided a more comprehensive view of longitudinal patterns in three GHGs across the upper, middle, and lower reaches affected by different types and magnitudes of anthropogenic perturbations (Figs. 2–4). All three GHGs exhibited large longitudinal variations associated with gas-specific increases at impoundment-affected sites and localized pulses along the lower reach downstream of polluted urban tributary inflows. Although pCO_2 at some impoundment-affected sites was very low, approaching or falling below the atmospheric equilibrium, three GHGs were generally supersaturated with respect to the atmosphere across the river basin (Table 1; Fig. 2). Very high levels of pCO_2 observed in the lower reach of the Han River (up to 4132 µatm) and its three urban tributaries (up to 11970 µatm) fall in the high ranges found in some polluted rivers in Europe (Kempe, 1984; Frankignoulle et al., 1998; Borges et al., 2006) and China (Yao et al., 2007; Ran et al., 2015; Liu et al., 2016; Wang et al., 2017). Consistent with these previous reports on pCO_2 and other studies reporting high levels of CH_4 and N_2O in polluted urban waters (Garnier et al., 2013; Yu et al., 2013; Smith et al., 2017; Wang et al., 2017b, 2018), the results observed in this

study emphasize the dominant influence of urban tributaries carrying wastewater as a primary anthropogenic source of GHGs in the highly urbanized river system.

Different longitudinal patterns in three GHGs (Fig. 2), together with reach-specific significant correlations between GHGs and other measured water quality components (Fig. 5; Table S4), illustrate that the spatial distribution and temporal dynamics of three GHGs in the Han River basin may be significantly different from those found in natural or less impacted river systems. While the extent of major natural sources such as wetlands and floodplains has been considered as the primary factor for longitudinal variations in CO_2 and CH_4 in large rivers (Richey et al., 1988; Borges et al., 2013; Abril et al., 2014), the lack of these natural sources, along with the distinct patterns of GHGs attributed to dams and urban wastewater, suggests that altered water retention time and nutritional status might exert critical controls on the production and consumption of three GHGs in this highly regulated river system (Crawford et al., 2016). It would be very challenging to tease out multiple, interrelated factors as shown by previous studies of GHG dynamics in urbanized river systems (Smith et al., 2017; Wang et al., 2017b). However, the observed longitudinal patterns of three GHGs (Figs. 2–4), along with their correlations with specific sets of water quality components (Fig. 5), make one thing clear. The primary factors and mechanisms for the production and consumption of three GHGs may change in response to longitudinal variations in dominant anthropogenic perturbations, often abruptly as shown by the localized pulses of GHGs downstream of urban tributary inflows (Figs. 2, 8).

Spatial variations in three GHGs observed along the middle reach (Figs. 2 – 4) suggest that complex interacting metabolic processes in water column and sediment influence the levels of three GHGs to varying degrees depending on gas and reservoir. Lower values of pCO_2 measured at all impoundment-affected sites including site HR11 downstream of the last dam (HR10) indicate an enhanced planktonic CO_2 uptake, in agreement with enhanced photosynthesis and lowered pCO_2 levels observed in some eutrophic impounded reaches of the Mississippi (Crawford et al., 2016), the Yangtze (Liu et al., 2016), and a Yellow River tributary (Ran et al., 2017). However, other studies have reported drastic increases in CO_2 and CH_4 emissions from the flooded vegetation and soils in the early years following dam construction (Abril et al., 2005; Chen et al., 2009; Shi et al., 2017). Given the negative relationship established between reservoir age and emissions of CO_2 and CH_4 from a wide range of hydroelectric reservoirs (Barros et al., 2011), pulses of GHGs from the newly constructed reservoirs might taper gradually with increasing reservoir age. Unlike other studies that have reported significant negative relationships between Chl a and pCO_2 in eutrophic impounded rivers (Crawford et al., 2016; Liu et al., 2016; Ran et al., 2017), pCO_2 was not correlated with Chl a in the middle reach, but had some significant positive correlations with DOM optical properties such as HIX, C1/DOC, and C2/DOC (Fig. 4), which may be associated with terrestrial DOM components and their microbial transformation products (Fellman et al., 2010; Parr et al., 2015). It is likely that the narrow ranges of pCO_2 and Chl a did not result in any significant correlation. However, the concurrence in the relatively high levels of pCO_2 and DOC moieties of terrestrial origin at some middle reach sites that are less affected by impoundments (e.g., HR 7 and HR8) might have resulted in the observed significant correlations.

Although a small number of measurements of CH_4 and N_2O and their inconsistent spatial patterns observed along the impounded middle reach (Fig. 2; Tables S2, S3) require a cautious assessment of dam effects, the higher values of CH_4 and

N₂O measured in some dams and outflows compared to upstream levels indicate dam-specific conditions driving the production and consumption of CH_4 and N_2O in reservoir water or sediments. Crawford et al (2016) observed a weak summer-time CO_2 sink due to enhanced photosynthesis but elevated concentrations and fluxes of CH_4 along the upper Mississippi River reaches impounded by a series of low-head dams. They attributed the observed supersaturation in CH_4 to anaerobic conditions in organic-rich sediments. Despite no correlation between CH_4 and DO levels in the middle reach (Fig. 5; Table S4), the fact that CH_4 levels were higher at three shallower dam sites (HR6, HR7, and HR10) than at the most upstream dam (HR5), which is very deep with a maximum depth reaching 110 m, implies the balance between anaerobic CH_4 production in bottom sediment and aerobic and anaerobic CH_4 oxidation in water column with a depth-dependent gradient of O_2 availability as a driving force for the observed spatial variations (Roland et al., 2017). Shallow reservoirs and river inflows accumulating methanogenic sediments have been identified as CH_4 emission hot spots in impounded river systems due to comparatively low rates of CH_4 oxidation in aerobic water column (Maeck et al., 2013; Beaulieu et al., 2014). The significant correlation between CH_4 and DOC (Figs. 4, 5) is consistent with other studies relating DOC to CH_4 conversion in reservoirs based on the coupling between anaerobic organic matter degradation and methanogenesis (Chen et al., 2009; Wang et al., 2017b). As noted by Bergier et al. (2014), organic wastes released from local sources might also have contributed to the transformation of DOC to CH_4. Higher CH_4 concentrations measured at warmer temperatures are also in agreement with the higher rates of CH_4 production observed during warm summer months in a shallow reservoir in Ohio, USA (Beaulieu et al., 2014). N enrichment, alone or in combination with anaerobic conditions favourable for denitrification, has been suggested as the key control on N_2O production in impoundments, although strictly anaerobic conditions might result in a more complete denitrification to N_2, contributing little to N_2O production (Beaulieu et al., 2015; Wang et al., 2017b). The lack of clear dam effects on N_2O except for one dam site (HR6; Fig. 2) might be explained by the complex interactions between microbial N transformations in the oxygen-rich epilimnion and oxygen-poor hypolimnion (Beaulieu et al., 2015).

Large increases in GHG concentrations along the lower reach might be explained by a suite of related processes including in-stream metabolisms and direct inputs from WWTPs. Direct influences of wastewater-derived GHGs have been observed in urban rivers receiving WWTP effluents (Garnier et al., 2013; Yu et al., 2013; Burgos et al., 2015; Alshboul et al., 2016; Wang et al., 2017a; Yoon et al., 2017). For example, large pulses of CH_4 and N_2O in the Guadalete River estuary in Spain were found near the discharge from a WWTP, as a combined result of direct gas emissions from WWTP effluents and indirect effects on the production of CH_4 and N_2O in the water channel and benthic sediments downstream (Burgos et al., 2015). Previously we used a mass balance approach based on three cruise underway measurements of pCO_2 to show that two tributaries JN and TC delivering WWTP effluents accounted for 72% of the CO_2 concentration measured at a downstream location in the lower Han River (Yoon et al., 2017). When the estimated rates of CO_2 production, consumption, and outgassing along the downstream reach were compared in June 2016, the amount of CO_2 produced from organic matter biodegradation was much greater than the amount of CO_2 consumed by phytoplankton and similar to the CO_2 efflux to the atmosphere. In May 2015, when Chl a concentrations were much higher than in June 2016, the bulk of CO_2 delivered by the tributaries was estimated to be consumed by phytoplankton photosynthesis along the same reach. As observed in other polluted rivers enriched in labile DOM moieties

derived from urban sewage (Guo et al., 2015), newly produced CO_2 from active microbial decomposition can sometimes exceed the phytoplankton uptake of CO_2 depending on the prevailing environmental conditions. By directly measuring $\delta^{13}C$ in CO_2 respired by bacterioplankton across a gradient of streams and lakes in Canada, McCallister and del Giorgio (2008) showed that the production of CO_2 through bacterial degradation of terrigenous DOM decreased in sharp contrast to the increasing proportion of algal-derived DOC and CO_2 with increasing levels of Chl a. Their findings implied an algal-driven activation of metabolism in eutrophic freshwater systems. However, it remains largely unexplored how the balance between autotrophy and heterotrophy in eutrophic river systems shifts in response to changing environmental conditions (Garnier and Billet, 2007).

Large down-river increases (Fig. 2) and temporal variability (Figs. 3, S1) in CH_4 and N_2O along the lower reach may result from a combination of processes including direct WWTP discharge and in-stream production and consumption. As indicated by the similar ranges of two gases found in the WWTP effluents and the tributary JN outlet (Fig. 6), the amount of CH_4 and N_2O discharged from the WWTP appeared to drive the magnitude and temporal variability of the tributary inputs to the lower reach. In the case of CH_4, however, the large spatial and temporal variations observed along the tributary upstream of the WWTP also point to the potential role of the benthic sediment as an upstream source of CH_4 (Stanley et al., 2016), although further research is needed to elucidate all important sources of the tributary CH_4. Despite the dominant influence of tributary exports, other riverine processes also need to be considered to explain the complex downstream spatial patterns of these gases, as indicated by the gas-specific sets of significant correlations with measured water quality components (Fig. 5). In contrast to the lacking or weak correlations indicative of anaerobic CH_4 production in the impounded middle reach, CH_4 measurements in the lower reach exhibited significant negative (DO) or positive (water temperature, C1/DOC, and C2/DOC) correlations related to anaerobic metabolism. As observed in other urbanized river systems (Beaulieu et al., 2015; Smith et al., 2015; Wang et al., 2018), eutrophication (indicated by significant positive correlation with PO_4^{3-}), together with lowered DO, might create favourable conditions for anaerobic methanogenesis in the lower reach almost impounded by two submerged weirs. Out of many water quality components that were significantly correlated with N_2O (Fig. 5), NH_4^+ and NO_3^- have been considered as two primary predictors of riverine N_2O, particularly in urban streams and rivers influenced by sewage (Yu et al., 2013, He et al., 2017; Smith et al., 2017). The lack of significant correlation with DO in the lower reach may indicate nitrification overweighing denitrification as the dominant process of N_2O production, although we cannot exclude the role of anaerobic N_2O production given the significant negative relationship between DO and N_2O data for the whole Han River basin (Fig. 4).

4.2 Tracking sources of DOM and GHGs using C isotopes

The dual C isotope ratios in DOM measured at five monthly monitoring sites, the tributary JN outlet, and an adjacent WWTP discharge fall within the ranges associated with soil organic matter (SOM) and phytoplankton biomass (Fig. 7; Raymond and Bauer, 2001; Marwick et al., 2015 and references therein). When Marwick et al. (2015) compared 695 measurements of $\Delta^{14}C_{DOC}$ in a wide range of global river systems, most data fell in the range from −100 to +200‰, with 72% of the data indicating a modern age compared to the much smaller proportion of modern POC (22% of 483 POC data). The relatively

large between-site variations in both $\delta^{13}C_{DOC}$ and $\Delta^{14}C_{DOC}$ make it very difficult to evaluate the relative contributions of allochthonous and autochthonous sources to the isotopic signatures of the bulk DOM. In particular, large fluctuations in $\delta^{13}C_{DOC}$ along the upper to middle reaches from HR2 to HR11 do not present any consistent longitudinal trend of the stable C isotopic composition. However, distinct increases in $\delta^{13}C_{DOC}$ at the most downstream site (HR14) compared to the $\delta^{13}C_{DOC}$ at the forested headwater stream (HR1) indicate a potential contribution of autochthonous DOM components to the isotopic signature of the bulk riverine DOM, which deviated substantially from those of the headwater DOM dominated by allochthonous components (Fig. 7). In addition, the distinct seasonal differences in isotopic signatures suggest that the age of DOM is generally younger at five mainstem sites across the river basin during the monsoon period (July 2014; modern − 590 years B.P.) than in the dry season (May 2015; 180 − 675 years B.P.) (Fig. 7). This seasonality might have resulted from an increased contribution of DOM moieties released from terrestrial sources during monsoon rainfalls. The enrichment of DOC in ^{14}C identified in other temperate river systems has been attributed to a larger contribution from ^{14}C-enriched litter and soil organic matter and shorter residence times of DOM in systems with higher annual precipitation (Raymond and Bauer, 2001; Butman et al., 2015). The latitudinal decreases in Δ^{14}C along the mainstem toward the values found in the urban tributary and WWTPs point to the dominant contribution of DOM derived from anthropogenic sources. The values of $^{13}C_{DOC}$ (−25.8‰) and $\Delta^{14}C_{DOC}$ (−97.9‰, −113.5‰) measured in WWTP effluents (Table S6) were similar to those reported by other studies (Griffith et al., 2009; Butman et al., 2015). As suggested by Griffith and Raymond (2011), aged DOM moieties in WWTP effluents (765 − 905 years B.P.; Table S6) may not only leave clear isotopic signatures on DOM in downstream reaches, but also fuel the riverine heterotrophy by providing labile sources for biodegradation.

The longitudinal increase in $\delta^{13}C_{CO2}$ from −20.9‰ at 76 km from the river mouth to −16.7‰ at 50 km from the river mouth in Fig. 8 might be related to a complex array of interacting processes such as organic matter degradation, photosynthesis by phytoplankton, and atmospheric gas exchange, which have usually been investigated as determinants of the isotopic composition of riverine DIC consisting of dissolved CO_2, bicarbonate, and carbonate (Barth et al., 2003; Schulte et al., 2011; Zeng et al., 2011; Deirmendjian and Abril, 2018). The observed values of $\delta^{13}C_{CO2}$ fall within the reported ranges of δ^{13}C measured for CO_2 dissolved in riverine and estuarine waters (−25 − −15‰) (Longinelli and Edmond, 1983; Maher et al., 2013). However, the values reported here are less negative than the ranges of δ^{13}C measured directly for CO_2 respired by bacteria consuming organic matter of terrestrial and algal origin in two streams and eight lakes in Canada (−32.5 − −28.4‰) (McCallister and del Giorgio, 2008). When the observed values of $\delta^{13}C_{CO2}$ are compared with the low range of $\delta^{13}C_{CO2}$ reported by McCallister and del Giorgio (2008) and the usual ranges of δ^{13}C in plant and algal biomass as two primary biological sources of riverine CO_2 (Fig. 7), it follows then that other riverine processes than bacterial degradation of plant (predominantly C3 in the studied basin) and algal biomass might be involved in the upward shift of $\delta^{13}C_{CO2}$. It has been reported that δ^{13}C in riverine DIC derived from carbonate dissolution and bacterial respiration ranges from −15 − −5‰, reflecting the balance between the concurrent processes that can either enrich or deplete DIC in ^{13}C (Telmer and Veizer et al., 1999; Barth et al., 2003; Schulte et al., 2011; Zeng et al., 2011). In contrast to the preferential use of the lighter organic C by heterotrophic bacteria

depleting ^{13}C in the respired CO_2, photosynthesis and atmospheric gas exchange can result in an enrichment of ^{13}C in remaining riverine CO_2 through preferential phytoplankton uptake of the lighter $^{12}CO_2$ and dissolution of atmospheric CO_2 enriched in ^{13}C, respectively (Schulte et al., 2011).

Assuming an enrichment of 10 ‰ from dissolved CO_2 to DIC (McCallister and del Giorgio, 2008), with a caution in mind that the actual $\delta^{13}C$ in DIC might be determined by various factors including initial concentrations and isotopic ratios of each DIC species and complex processes producing or consuming those DIC species (Deirmendjian and Abril, 2018), the estimated $\delta^{13}C$ in DIC (−11 – −7‰) would fall within the usual ranges found in global river systems (Schulte et al., 2011). The 4‰ down-river increase in $\delta^{13}C_{CO2}$ concurred with general increases in Chl a along the lower reach flanked by two submerged weirs (69 – 50 km from the river mouth) (Fig. 8), implying primary production as an important factor affecting the isotopic composition of dissolved CO_2 in the eutrophic reach. The enrichment of CO_2 in ^{13}C along the reaches downstream of the urban tributaries also indicates a significant contribution from urban tributaries enriched in ^{13}C (TC: –18.3‰; JN: –18.2‰; AY: –14.7 ‰) relative to the upstream value (–20.9‰) (Table S8). The distinctively higher values of $\delta^{13}C$ observed for the tributary CO_2 might have resulted from a combination of processes, including the same photosynthesis and atmospheric gas exchange as occurring in the mainstem and tributary-specific processes such as the transport and transformations of anthropogenic organic matter in urban wastewater. WWTP effluents have been shown to contain old organic matter with characteristic C isotopic composition (Griffith et al., 2009; Griffith and Raymond, 2011; Butman et al., 2015). Another potential source of isotopic enrichment might be the production of CH_4 from the reduction of CO_2 in the deeper water and bottom sediment, which consumes lighter C resulting in an enrichment of the remaining DIC pool (Barth et al., 2003). However, this mechanism might be less important than other described processes, because the latitudinal increase in $\delta^{13}C$ in CH_4 (Fig. 8) indicates an active oxidation occurring through the shallow downstream reach.

While agricultural activities, including rice cultivation, animal husbandry, and N fertilization, represent the primary anthropogenic source of CH_4 and N_2O in anthropogenically impacted river systems (Silvennoinen et al., 2008; Garnier et al., 2013), the relative contribution of wastewater and landfills often increases drastically in urbanized watersheds (Yu et al., 2013; Smith et al., 2017; Wang et al., 2017b). Downstream changes in CH_4 concentrations along the lower reach reflect localized impacts of urban tributary inputs, which caused pulsatile increases in the mainstem CH_4 concentrations and decreases in $\delta^{13}C$ in CH_4 downstream of the tributary inflow (Fig. 8). The concentrations of CH_4 peaked downstream of the tributary inflow, but gradually decreased along the downstream reach, indicating efficient CH_4 oxidation and/or evasion of CH_4 to the atmosphere. Similar localized effects of WWTP effluents were observed in the lower reaches of Seine River, downstream of Paris and Rouen, France (Garnier et al., 2013). Down-river concentration decreases and ^{13}C enrichment in CH_4 are consistent with the underway measurements conducted using a cavity ring-down spectroscopy(CRDS) along a 15 km reach of the North Creek estuary in Australia, which displayed CH_4 concentrations and $\delta^{13}C$ values ranging from 2 to 74 nmol and −61.07 to −48.62‰, respectively (Maher et al., 2013). While CH_4 oxidation was suggested as the primary driver of downstream increases in $\delta^{13}C$ in the estuary with relatively low levels of anthropogenic pollution (Maher et al., 2013), the down-river patterns of CH_4 concentration and isotopic composition observed in this study may be better explained by combining tributary inputs of CH_4

with lower $\delta^{13}C$ values compared to the mainstem values with CH_4 oxidation in the well-mixed, shallow lower reach. Although we did not include N isotopes in tracing sources of N_2O, the approach combining measurements of $\delta^{13}C$ in CO_2 and CH_4 with the dual C isotope analyses of DOM was useful in tracking sources along the eutrophic lower reach receiving tributary inputs with distinct isotopic signatures.

5 Implications

The observed large longitudinal variations in GHGs and associated environmental variables suggest that the traditional view of river continuum assuming gradual changes in riverine metabolism and organic matter composition (Vannote et al., 1980) might have a limited validity in explaining the high spatial variability in three GHGs observed in this study. Although the river continuum concept has been useful in explaining gradual longitudinal variations in CO_2 from headwater streams to lowland rivers corresponding to the changing balance between autotrophy and heterotrophy (Borges and Abril, 2012; Koehler et al., 2012; Catalán et al., 2016; Hotchkiss et al., 2015), it has been increasingly recognized that rivers are often divided into discrete segments such as reaches impounded by dams (Ward and Stanford, 1983; Poole, 2002) and eutrophic reaches receiving wastewater (Garnier and Billen, 2007; Yoon et al., 2017; Park et al., 2018). The observed reach-specific patterns of altered water quality and GHG dynamics provide an empirical evidence for ecosystem structural and functional responses to anthropogenic changes in hydrogeomorphic patches of the fluvial landscape, which have been emphasized in recent conceptual models integrating fluvial geomorphology and ecosystem processes at the valley to reach scales (Thorp et al., 2010). Previous studies of DOM biodegradation have often assumed a selective degradation of labile components of riverine organic matter along the continuum with minimal to low levels of anthropogenic perturbations (Koehler et al., 2012; Weyhenmeyer et al., 2012; Catalán et al., 2016). Reach-specific significance levels observed for the correlations between GHGs and DOC or its optical properties (Fig. 5; Table S4) imply that autochthonous DOM in the impounded middle reach or the eutrophic lower reach and anthropogenic DOM moieties derived from agricultural runoff or urban wastewater can continue to replenish the riverine pool of DOM, fuelling the river heterotrophy. This enhanced heterotrophy, along with direct discharges of GHGs from WWTPs, may result in highly localized pulses of GHGs along the lower Han River and other eutrophic urban rivers worldwide. Estimated rates for the production (biodegradation) and consumption (photosynthesis) of CO_2 in the lower reach downstream of major tributary inflows differed substantially depending on hydroclimatic conditions and algal abundance, indicating a shifting balance between autotrophy and heterotrophy driving CO_2 dynamics (Yoon et al., 2017). Some potential activation of riverine metabolic processes was also indicated by gas-specific sets of significant correlations between gas concentrations and related water quality measurements shown for the lower reach (Fig. 5). The increased availability of P, together with DO and DOM optical characteristics indicative of humic-like and microbial humic-like DOM (HIX, C1/DOC, and C2/DOC), was associated with high levels of pCO_2 and CH_4, suggesting that P enrichment and subsequent enhancement of algal productivity and anaerobic metabolism may create favourable conditions for the production of both CO_2 and CH_4. In contrast, the levels of NH_4^+ and NO_3^-, rather than PO_4^{3-}, were significantly correlated with N_2O concentrations in the lower reach, in agreement with

520 the well established relationship between N levels and N_2O production mechanisms in eutrophic rivers affected by urban sewage (Beaulieu et al. 2010; Yu et al., 2013; He et al., 2017). Urban tributary effects on metabolic processes in the eutrophic lower reach were also reflected in the lower-reach values of $\delta^{13}C$ in CO_2 and CH_4 resembling those measured in the tributaries (Fig. 8).

Because the used statistical and chemical approaches can provide only indirect evidence of altering metabolic regimes in the
525 eutrophic urban river system, more process-focused research is required to elucidate dominant factors and mechanisms and evaluate the relative contributions of various metabolic processes and external supplies of GHGs derived from WWTP effluents. In the context of anthropogenic river discontinuum (Park et al., 2018), impoundments and urban water pollution might be coupled through hydrologic connection and hence cause synergistic effects on downstream metabolic processes. In the case of the Han River basin, old cascade dams on the North Han River and large weirs newly constructed on the South Han
530 River might be altering not only GHG dynamics but also DOM composition and transformations. It warrants further research to explore how dam-induced changes in water retention and C biogeochemistry cascade down to affect organic matter transformations and GHG emissions in the eutrophic lower reach. Identifying hot spots of water pollution and GHG emissions in highly human-impacted river systems would contribute to establishing novel river basin management options integrating the traditional water quality control and an emerging challenge of climate change mitigation by helping watershed managers
535 set priority areas of policy responses to multiple concurrent environmental stresses.

Data availability

More data are available in supplementary information and can be requested from the corresponding author (jhp@ewha.ac.kr).

Author contribution

All authors contributed to data acquisition, discussion, and manuscript preparation. Manuscript writing was coordinated by J.-
540 H. Park with contributions from all authors.

Competing interests

The authors declare that they have no conflict of interest.

Acknowledgements

This work was supported by the National Foundation of Korea (2014R1A2A2A01006577; 2017R1D1A1B06035179),
545 "Cooperative Research Program for Agriculture Science & Technology Development (PJ012489022018)" by Rural

Development Administration, Republic of Korea, and "Development of Gas Analysis Measurement Standards (18011051)" by Korea Research Institute of Standards and Science. We thank Borami Park for her assistance with sampling and analysis. We also thank three anonymous reviewers for their constructive and helpful comments.

References

550   Abril, G., Guérin, F., Richard, S., Delmas, R., Galy-Lacaux, C., Gosse, P., Tremblay, A., Varfalvy, L., Dos Santos, M. A., and Matvienko, B.: Carbon dioxide and methane emissions and the carbon budget of a 10-year old tropical reservoir (Petit Saut, French Guiana), Global Biogeochem. Cycles, 19, GB4007, doi:10.1029/2005GB002457, 2005.

Abril, G., Martinez, J.-M., Artigas, L. F., Moreira-Turcq, P., Benedetti, M. F., Vidal, L., Meziane, T., Kim, J.-H., Bernardes, M. C., Savoye, N., Deborde, J., Souza, E. L., Alberic, P., Landim de Souza, M. F., and Roland, F.: Amazon River carbon

555   dioxide outgassing fueled by wetlands, Nature, 505, 395–398, 2014.

Abril, G., Bouillon, S., Darchambeau, F., Teodoru, C. R., Marwick, T. R., Tamooh, F., Ochieng Omengo, F., Geeraert, N., Deirmendjian, L., Polsenaere, P., and Borges, A. V.: Technical Note: Large overestimation of pCO$_2$ calculated from pH and alkalinity in acidic, organic-rich freshwaters, Biogeosciences, 12, 67–78, 2015.

Alshboul, Z., Encinas-Fernandez, J., Hofmann, H., and Lorke, A.: Export of dissolved methane and carbon dioxide with

560   effluents from municipal wastewater treatment plants, Environ. Sci. Tech., 50, 5555–5563, doi:10.1021/acs.est.5b04923, 2016.

American Public Health Association: Standard Methods for the Examination of Water and Wastewater, American Public Health Association, Washington DC, 2005.

Barros, N., Cole, J. J., Tranvik, L. J., Prairie, Y. T., Bastviken, D., Huszar, V. L. M., del Giorgio, P., and Roland, F.: Carbon

565   emission from hydroelectric reservoirs linked to reservoir age and latitude, Nat. Geosci., 4, 593–596, doi:10.1038/ngeo1211, 2011.

Barth, J. A. C., Cronin, A. A., Dunlop, J., and Kalin, R.M.: Influence of carbonates on the riverine carbon cycle in an anthropogenically dominated catchment basin: evidence from major elements and stable carbon isotopes in the Lagan River (N. Ireland), Chem. Geo., 200, 203–216. doi:10.1016/S0009-2541(03)00193-1, 2003.

570   Bastviken, D., Tranvik, L. J., Downing, J. A, Crill, P. M., and Enrich-Prast, A.: Freshwater methane emissions offset the continental carbon sink, Science 331, 50, DOI: 10.1126/science.1196808, 2011.

Beaulieu, J. J., Shuster,W. D., and Rebholz, J. A.: Nitrous oxide emissions from a large, impounded river: the Ohio River, Environ. Sci. Technol., 44, 7527–7533, DOI: 10.1021/es1016735, 2010.

Beaulieu, J. J., Smolenski, R. L., Nietch, C. T., Townsend-Small, A., and Elovitz, M. S.: High methane emissions from a

575   midlatitude reservoir draining an agricultural watershed, Environ. Sci. Technol., 48, 11100–11108, doi:10.1021/es501871g, 2014.

Beaulieu, J. J., Nietch, C. T., and Young, J. L.: Controls on nitrous oxide production and consumption in reservoirs of the Ohio River Basin, J. Geophys. Res. Biogeosci., 120, doi:10.1002/2015JG002941, 2015.

Bergier, I., Ramos, F. M., and Bambace, L. A. W.: Dam reservoirs role in carbon dynamics requires contextual landscape ecohydrology, Environ. Monit. Assess., 186, 5985–5988, doi:10.1007/s10661-014-3834-2, 2014.

Borges, A. V., and Abril, G.: Carbon dioxide and methane dynamics in estuaries, in: Treatise on Estuarine and Coastal Science, Volume 5, Wolanski, E., and McLusky, D. (Eds.), Academic Press, Waltham, 119–161, doi:10.1016/B978-0-12-374711-2.00504-0, 2011.

Borges, A. V., Schiettecatte, L.-S., Abril, G., Delille, B., and Gazeau, F.: Carbon dioxide in European coastal waters, Estuar. Coast. Shelf Sci., 70, 375–387, doi:10.1016/j.ecss.2006.05.046, 2006.

Borges, A. V., Darchambeau, F., Teodoru, C. R., Marwick, T. R., Tamooh, F., Geeraert, N., Omengo, F. O., Guérin, F., Lambert, T., Morana, C., Okuku, E., and Bouillon, S.: Globally significant greenhouse gas emissions from African inland waters, Nat. Geosci., 8, 637–642, doi:10.1038/NGEO2486, 2015.

Borges, A.V., Darchambeau, F., Lambert, T., Bouillon, S., Morana, C., Brouyère, S., Hakoun, V., Jurado, A., Tseng, H.-C., Descy, J.-P., Roland, F.A.E.: Effects of agricultural land use on fluvial carbon dioxide, methane and nitrous oxide concentrations in a large European river, the Meuse (Belgium), Sci. Total Environ., 610–611, 342-355, doi:10.1016/j.scitotenv.2017.08.047, 2018.

Burgos, M., Sierra, A., Ortega, T., and Forja, J. M.: Anthropogenic effects on greenhouse gas (CH_4 and N_2O) emissions in the guadalete river estuary (SW Spain), Sci. Total Environ., 503–504, 179–189, doi:10.1016/j.scitotenv.2014.06.038, 2015.

Butman, D. E., Wilson, H. F., Barnes, R. T., Xenopoulos, M. A., and Raymond, P. A.: Increased mobilization of aged carbon to rivers by human disturbance, Nat. Geosci., 8, 112–116, doi:10.1038/ngeo2322, 2015.

Catalán, N., Marcé R., Kothawala, D. N., and Tranvik, L. J.: Organic carbon decomposition rates controlled by water retention time across inland waters, Nat. Geosci., 9, 501–504, doi:10.1038/ngeo2720, 2016.

Chen, H., Wu, Y., Yuan, X., Gao, Y., Wu, N., and Zhu, D.: Methane emissions from newly created marshes in the drawdown area of the Three Gorges Reservoir, J. Geophys. Res., 114, D18301, doi:10.1029/2009JD012410, 2009.

Cole, J. J., Prairie, Y. T., Caraco, N. F., McDowell, W. H., Tranvik, L. J., Striegl, R. G., Duarte, C. M., Kortelainen, P., Downing, J. A., Middelburg, J. J., and Melack, J.: Plumbing the global carbon cycle: Integrating inland waters into the terrestrial carbon budget, Ecosystems, 10, 171–184, doi:10.1007/s10021-006-9013-8, 2007.

Crawford, J. T., Loken,L. C., Stanley, E. H., Stets, E. G., Dornblaser,M. M., and Striegl, R. G.: Basin scale controls on CO_2 and CH_4 emissions from the Upper Mississippi River, Geophys. Res. Lett., 43, 1973–1979, doi:10.1002/2015GL067599, 2016.

Fellman, J. B., Hood, E., and Spencer, R. G. M.: Fluorescence spectroscopy opens new windows into dissolved organic matter dynamics in freshwater ecosystems: A review, Limnol. Oceanogr., 55, 2452–2462, doi:10.4319/lo.2010.55.6.2452, 2010.

Frankignoulle, M., Abril, G., Borges, A., Bourge, I., Canon, C., Delille, B., Libert, E., and Théate, J.-M.: Carbon dioxide emission from European estuaries, Science, 282, 434–436, doi:10.1126/science.282.5388.434, 1998.

Garnier, J. and Billen, G.: Production vs. Respiration in river systems: An indicator of an "ecological status", Sci. Total Environ., 375, 110–124, doi:10.1016/j.scitotenv.2006.12.006, 2007.

Garnier, J., Vilain, G., Silvestre, M., Billen, G., Jehanno, S., Poirier, D., Martinez, A., Decuq, C., Cellier, P., and Abril, G.: Budget of methane emissions from soils, livestock and the river network at the regional scale of the Seine basin (France), Biogeochemistry, 116, 199–214, doi:10.1007/s10533-013-9845-1, 2013.

Gran, G.: Determination of the equivalence point in potentiometric titrations. Part II, Analyst, 77, 661–671, doi:10.1039/AN9527700661, 1952.

Griffith, D. R., Barnes, R. T., and Raymond, P. A.: Inputs of fossil carbon from wastewater treatment plants to U.S. rivers and oceans, Environ. Sci. Technol., 43, 5647–5651, doi:10.1021/es9004043, 2009.

Griffith, D. R., and Raymond, P. A.: Multiple-source heterotrophy fueled by aged organic carbon in an urbanized estuary, Mar. Chem., 124, 14–22, doi:10.1016/j.marchem.2010.11.003, 2011.

Guo, W., Yang, L., Zhai, W., Chen, W., Osburn, C. L., Huang, X., and Li, Y.: Runoff-mediated seasonal oscillation in the dynamics of dissolved organic matter in different branches of a large bifurcated estuary – The Changjiang Estuary, J. Geophys. Res. Biogeosci., 119, 776–793, doi:10.1002/2013JG002540, 2014.

He, Y., Wang, X., Chen, H., Yuan, X., Wu, N., Zhang, Q., Yue, J., Zhang, Q., Diao, Y., Zhou, L.: Effect of watershed urbanization on N_2O emissions from the Chongqing metropolitan river network, China, Atmos. Environ., 171, 70–81, doi:10.1016/j.atmosenv.2017.09.043, 2017.

Hotchkiss, E. R., Hall Jr, R. O., Sponseller, R. A., Butman, D., Klaminder, J., Laudon, H., Rosvall, M., and Karlsson, J.: Sources of and processes controlling CO_2 emissions change with the size of streams and rivers, Nat. Geosci., 8, 696–699, doi:10.1038/ngeo2507, 2015.

Hu, Y. and Cheng, H.: The urgency of assessing the greenhouse gas budgets of hydroelectric reservoirs in China, Nat. Clim. Change, 3, 708–712, doi:10.1038/nclimate1831, 2013.

Hudson, F.: Sample preparation and calculations for dissolved gas analysis in water samples using GC headspace equilibration technique, RSKSOP-175, Revision No. 2, U.S. Environmental Protection Agency, USA, 2004.

Jin, H., Yoon, T. K., Lee, S.-H., Kang, H., Im, J., and Park, J.-H.: Enhanced greenhouse gas emission from exposed sediments along a hydroelectric reservoir during an extreme drought event, Environ. Res. Lett., 11, 124003, doi:10.1088/1748-9326/11/12/124003, 2016.

Jung, B.-J., Lee, H.-J., Jeong, J.-J., Owen, J., Kim, B., Meusburger, K., Alewell, C., Gebauer, G., Shope, C., and Park, J.-H.: Storm pulses and varying sources of hydrologic carbon export from a mountainous watershed, J. Hydrol., 440–441, 90-101, doi:10.1016/j.jhydrol.2012.03.030, 2012.

Kaushal, S. S., and Belt, K. T.: The urban watershed continuum: evolving spatial and temporal dimensions, Urban Ecosyst., 15, 409–435, doi:10.1007/s11252-012-0226-7, 2012.

Kempe, S.: Sinks of the anthropogenically enhanced carbon-cycle in surface fresh waters, J. Geophys. Res., 89, 4657–4676, doi:10.1029/JD089iD03p04657, 1984.

645 Kling, G., Kipphut, G., and Miller, M.: The flux of CO_2 and CH_4 from lakes and rivers in arctic Alaska, Hydrobiologia, 240, 23–36, doi:10.1007/BF00013449, 1992.

Koehler, B., von Wachenfeldt, E., Kothawala, D., and Tranvik, L. J.: Reactivity continuum of dissolved organic carbon decomposition in lake water, J. Geophys. Res., 117, G01024, doi:10.1029/2011JG001793, 2012.

Lauerwald, R., Laruelle, G. G., Hartmann, J., Ciais, P., and Regnier, P. A. G.: Spatial patterns in CO_2 evasion from the global river network, Global Biogeochem. Cycles, 29, 534–554, doi:10.1002/2014GB004941, 2015.

Liu, S., Lu, X. X., Xia, X., Zhang, S., Ran, L., Yang, X., and Liu, T.: Dynamic biogeochemical controls on river pCO_2 and recent changes under aggravating river impoundment: An example of the subtropical Yangtze River, Global Biogeochem. Cycles, 30, 880–897, doi:10.1002/2016GB005388, 2016.

Longinelli, A. and Edmond, J. M.: Isotopic geocehmistry of the Amazon basin: A reconnaissance, J. Geophys. Res., 88, 3703–3717, doi:10.1029/JC088iC06p03703, 1983.

Maavara, T., Lauerwald, R., Regnier, P., and Van Cappellen, P.: Global perturbation of organic carbon cycling by river damming, Nat. Commun., 15347, doi:10.1038/ncomms15347, 2017.

Maeck, A., DelSontro, T., McGinnis, D. F., Fischer, H., Flury, S., Schmidt, M., Fietzek, P., and Lorke, A.: Sediment trapping by dams creates methane emission hot spots, Environ. Sci. Technol., 47, 8130–8137, doi:10.1021/es4003907, 2013.

660 Maher, D. T., Santos, I. R., Leuven, J. R. F. W., Oakes, J. M., Erler, D. V., Carvalho, M. C., and Eyre, B. D.: Novel use of cavity ring-down spectroscopy to investigate aquatic carbon cycling from microbial to ecosystem scales, Environ. Sci. Technol., 47, 12938–12945, doi:10.1021/es4027776, 2013.

Marx, A., Dusek, J., Jankovec, J., Sanda, M., Vogel, T., van Geldern, R., Hartmann, J., and Barth, J. A. C.: A review of CO_2 and associated carbon dynamics in headwater streams: A global perspective, Rev. Geophys., 55, 560–585, doi:10.1002/2016RG000547, 2017.

Marwick, T. R., Tamooh, F., Teodoru, C. R.,. Borges, A. V, Darchambeau, F., and Bouillon, S.: The age of river-transported carbon: A global perspective, Global Biogeochem. Cycles, 29, 122–137, doi:10.1002/2014GB004911, 2015.

McCallister, S. L. and del Giorgio, P. A.: Direct measurement of the $\delta^{13}C$ signature of carbon respired by bacteria in lakes: Linkages to potential carbon sources, ecosystem baseline metabolism, and CO_2 fluxes, Limnol. Oceanogr., 53, 1204–1216, doi:10.4319/lo.2008.53.4.1204, 2008.

McKnight, D. M., Boyer, E. W., Westerhoff, P. K., Doran, P. T., Kulbe, T., and Anderson, D. T.: Spectroflourometric characterization of dissolved organic matter for indication of precursor organic material and aromaticity, Limnol. Oceanogr., 46, 38–48, doi:10.4319/lo.2001.46.1.0038, 2001.

Min, D., Kang, N., Moon, D. M., Lee, J. B., Lee, D. S., and Kim, J. S.: Effect of variation in argon content of calibration gases on determination of atmospheric carbon dioxide, Talanta, 80, 422–427, doi:10.1016/j.talanta.2009.03.019, 2009.

Ministry of Environment: Statistics of Sewerage, Ministry of Environment, Sejong, Republic of Korea, 2015.

Park, J.-H., Duan, L., Kim, B., Mitchell, M. J., and Shibata, H.: Potential effects of climate change and variability on watershed biogeochemical processes and water quality in Northeast Asia, Environ. Int., 36, 212–225,

doi:10.1016/j.envint.2009.10.008, 2010.

680   Park, J.-H., Nayna, O. K., Begum, M. S., Chea, E., Hartmann, J., Keil, R. G., Kumar, S., Lu, X., Ran, L., Richey, J. E.,
Sarma, V. V. S. S., Tareq, S. M., Xuan, D. T., and Yu, R.: Reviews and syntheses: Anthropogenic perturbations to carbon fluxes in Asian river systems – concepts, emerging trends, and research challenges, Biogeosciences, 15, 3049–3069, doi:10.5194/bg-15-3049-2018, 2018.

Parr, T. B., Cronan, C. S., Ohno, T., Findlay, S. E. G., Smith, S. M. C. and Simon, K. S.: Urbanization changes the
685   composition and bioavailability of dissolved organic matter in headwater streams, Limnol. Oceanogr., 60(3), 885–900, doi:10.1002/lno.10060, 2015.

Poole, G. C.: Fluvial landscape ecology: addressing uniqueness within the river discontinuum, Freshwater Biol., 47, 641–660, doi:10.1046/j.1365-2427.2002.00922.x, 2002.

R Development Core Team: R: A language and environment for statistical computing; R Foundation for Statistical Computing:
690   Vienna, Austria, available at: http://www.r-project.org (last access: 1 June 2018), 2018.

Ran, L., Lu, X. X., Richey, J. E., Sun, H., Han, J., Liao, S., and Yi, Q.: Long-term spatial and temporal variation of CO_2 partial pressure in the Yellow River, China, Biogeosciences, 12, 921-932, doi:10.5194/bg-12-921-2015, 2015.

Ran, L., Li, L., Tian, M., Yang, X., Yu, R., Zhao, J., Wang, L., and Lu, X. X.: Riverine CO_2 emissions in the Wuding River catchment on the Loess Plateau: Environmental controls and dam impoundment impact, J. Geophys. Res. Biogeosci., 122,
695   1439–1455, doi:10.1002/2016JG003713, 2017.

Raymond, P. A. and Bauer, J. E.: Use of ^{14}C and ^{13}C natural abundances for evaluating riverine, estuarine, and coastal DOC and POC sources and cycling: a review and synthesis, Organic Geochemistry, 32, 469–485, doi:10.1016/S0146-6380(00)00190-X, 2001.

Raymond, P. A., Hartmann, J., Lauerwald, R., Sobek, S., McDonald, C., Hoover, M., Butman, D., Striegl, R., Mayorga, E.,
700   Humborg, C., Kortelainen, P., Dürr, H., Meybeck, M., Ciais, P., and Guth, P.: Global carbon dioxide emissions from inland waters, Nature, 503, 355–359, doi:10.1038/nature12760, 2013.

Regnier, P., Friedlingstein, P., Ciais, P., Mackenzie, F. T., Gruber, N., Janssens, I. A., Laruelle, G. G., Lauerwald, R., Luyssaert, S., Andersson, A. J., Arndt, S., Arnosti, C., Borges, A. V., Dale, A. W., Gallego-Sala, A., Goddéris, Y., Goossens, N., Hartmann, J., Heinze, C., Ilyina, T., Joos, F., LaRowe, D. E., Leifeld, J., Meysman, F. J. R., Munhoven, G., Raymond,
705   P. A., Spahni, R., Suntharalingam, P., and Thullner, M.: Anthropogenic perturbation of the carbon fluxes from land to ocean, Nat. Geosci., 6, 597–607, doi:10.1038/ngeo1830, 2013.

Richey, J. E., Devol, A. H., Wofsy, S. C., Victoria, R., and Riberio, M. N. G.: Biogenic gases and the oxidation and reduction of carbon in Amazon River and floodplain waters, Limnol. Oceanogr., 33, 551–561. Doi:10.4319/lo.1988.33.4.0551, 1988.

710   Roland, F. A. E., Darchambeau, F., Morana, C., Bouillon, S., Borges, A. V.: Emission and oxidation of methane in a meromictic, eutrophic and temperate lake (Dendre, Belgium), Chemosphere, 168, 756–764, doi:10.1016/j.chemosphere.2016.10.138, 2017.

Schulte, P., van Geldern, R., Freitag, H., Karim, A., Négrel, P., Petelet-Giraud, E., Probst, A., Probst, J.-L., Telmer, K, Veizer, J., and Barth, J. A. C.: Applications of stable water and carbon isotopes in watershed research: weathering, carbon cycling, and water balances, Earth Sci. Rev., 109, 20–31, doi:10.1016/j.earscirev.2011.07.003, 2011.Seoul Metropolitan Government: The 8th Han River Ecosystem Survey, Seoul Institute, Seoul, Republic of Korea, 2017.

Shi, W., Chen, Q., Yi, Q., Yu, J., Ji, Y., Hu, L., and Chen, Y.: Carbon emission from cascade reservoirs: Spatial heterogeneity and mechanisms, Environ. Sci. Technol., 51, 12175–12181, doi:10.1021/acs.est.7b03590, 2017.

Silvennoinen, H., Liikanen, A., Rintala, J., and Martikainen, P. J.: Greenhouse gas fluxes from the eutrophic Temmesjoki river and its estuary in the Limganlahti Bay (the Baltic Sea), Biogeochemistry 90, 193–208, doi:10.1007/s10533-008-9244-1, 2008.

Smith, R. M., Kaushal, S. S., Beaulieu, J. J., Pennino, M. J., and Welty, C.: Influence of infrastructure on water quality and greenhouse gas dynamics in urban streams, Biogeosciences, 14, 2831–2849, doi:10.5194/bg-14-2831-2017, 2017.

Stanley, E. H., Casson, N. J., Christel, S., Crawford, J. T., Loken, L. C., and Oliver, S. K.: The ecology of methane in streams and rivers: patterns, controls, and global significance, Ecol. Monogr., 86, 146–171, doi:10.1890/15-1027.1, 2016.

Syvitski, J. P. M., Vörösmarty, C. J., Kettner, A. J., and Green, P.: Impact of humans on the flux of terrestrial sediment to the global coastal ocean, Science, 308, 376–380, doi:10.1126/science.1109454, 2005.

Telmer, K., Veizer, J.: Carbon fluxes, pCO_2 and substrate weathering in a large northern river basin, Canada: carbon isotope perspectives. Chem. Geol. 159, 61–86, doi:10.1016/S0009-2541(99)00034-0, 1999.

Teodoru, C. R., Nyoni, F. C., Borges, A. V., Darchambeau, F., Nyambe, I., and Bouillon, S.: Dynamics of greenhouse gases (CO_2, CH_4, N_2O) along the Zambezi River and major tributaries, and their importance in the riverine carbon budget, Biogeosciences, 12, 2431–2453, doi:10.5194/bg-12-2431-2015, 2015.

Thorp, J. H., Flotemersch, J. E., Delong, M. D., Casper, A. F., Thoms, M. C., Ballantyne, F., Williams, B. S., O'Neill, B. J., and Haase. C. S.: Linking ecosystem services, rehabilitation, and river hydrogeomorphology, BioScience, 59, 67–74, doi:10.1525/bio.2010.60.1.11, 2010.

Vannote, R. L., Minshall, G. W., Cummins, K. W., Sedell, J. R., and Cushing, C. E.: The river continuum concept, Can. J. Fish. Aquat. Sci., 37, 130–137, doi:10.1139/f80-017, 1980.

Wang, X., He, Y., Yuan, X., Chen, H., Peng, C., Zhu, Q., Yue, J., Ren, H., Deng, W., and Liu, H.: pCO_2 and CO_2 fluxes of the metropolitan river network in relation to the urbanization of Chongqing, China, J. Geophys. Res. Biogeocsi., 122, 470–486, doi:10.1002/2016JG003494, 2017a.

Wang, X., He, Y., Yuan, X., Chen, H., Peng, C., Yue, J., Zhang, Q., Diao, Y., Liu, S.: Greenhouse gases concentrations and fluxes from subtropical small reservoirs in relation with water shed urbanization, Atmos. Environ., 154, 225–235, doi:10.1016/j.atmosenv.2017.01.047, 2017b.

Wang, X., He, Y., Chen, H., Yuan, X., Peng, C., Yue, J., Zhang, Q., Zhou, L.: CH_4 concentrations and fluxes in a subtropical metropolitan river network: Watershed urbanization impacts and environmental controls, Sci. Total Environ., 622–623, 1079–1089, doi:10.1016/j.scitotenv.2017.12.054, 2018.

Ward, J. V. and Stanford, J. A.: Serial discontinuity concept of lotic ecosystems, in: Dynamics of Lotic Systems, Fontaine, T. D. and Bartell, S. M. (Eds.), Ann Arbor Science, Ann Arbor, 29–42, 1983.

Weishaar, J. L., Aiken, G. R., Bergamaschi, B. A., Fram, M. S., Fujii, R., and Mopper, K.: Evaluation of specific ultra-violet

750   absorbance as an indicator of the chemical composition and reactivity of dissolved organic carbon, Environ. Sci. Technol., 37, 4702–4708, doi:10.1021/es030360x, 2003.

Weyhenmeyer, G. A., Fröberg, M., Karltun, E., Khalili, M., Kothawala, D., Temnerud, J., and Tranvik, L. J.: Selective decay of terrestrial organic carbon during transport from land to sea, Glob. Change Biol., 18, 349–355, doi:10.1111/j.1365-2486.2011.02544.x, 2012.

755 Yao, G., Gao, Q., Wang, Z., Huang, X., He, T., Zhang, Y., Jiao, S., and Ding, J.: Dynamics of CO_2 partial pressure and CO_2 outgassing in the lower reaches of the Xijiang River, a subtropical monsoon river in China, Sci. Total Environ., 376, 255–266, doi:10.1016/j.scitotenv.2007.01.080, 2007.

Yoon, T. K., Jin, H., Oh, N.-H., and Park, J.-H.: Technical note: Assessing gas equilibration systems for continuous pCO$_2$ measurements in inland waters, Biogeosciences, 13, 3915–3930, doi:10.5194/bg-13-3915-2016, 2016.

760 Yoon, T. K., Jin, H., Begum, M. S., Kang, N., and Park, J.-H.: CO_2 outgassing from an urbanized river system fueled by wastewater treatment plant effluents, Environ. Sci. Technol., 51, 10459–10467, doi:10.1021/acs.est.7b02344, 2017.

Yu, Z. J., Deng, H. G., Wang, D. Q., Ye, M. W., Tan, Y. J., Li, Y. J., Chen, Z. L., and Xu, S.Y.: Nitrous oxide emissions in the Shanghai river network: implications for the effects of urban sewage and IPCC methodology, Glob. Change Biol., 19, 2999–3010, doi:10.1111/gcb.12290, 2013.

765 Zeng, F.-W., Masiello, C. A., and Hockaday, W. C.: Controls on the origin and cycling of riverine dissolved inorganic carbon in the Brazos River, Texas, Biogeochemistry, 104, 275–291, doi:10.1007/s10533-010-9501-y, 2011.

Zsolnay, A., Baigar, E., Jimenez, M., Steinweg, B., and Saccomandi, F.: Differentiating with fluorescence spectroscopy the sources of dissolved organic matter in soils subjected to drying, Chemosphere, 38, 45–50, doi:10.1016/S0045-6535(98)00166-0, 1999.

Table 1. Summary of sampling sites and 3 GHGs measured in two basin-wide surveys at 15 sites and monthly monitoring from July 2014 to July 2015 at 6 sites in the Han River basin. Note that additional data obtained an urban tributary (HR 12) from May 2015 to December 2017 (N=13) are also presented as monthly data.

Reach	Site	Name	Description	Coordinates	Distance to mouth (km)	pCO_2 (µatm) Monthly	July 2014	May 2015	CH_4 (nmol L^{-1}) Monthly	May 2015	N_2O (nmol L^{-1}) Monthly	May 2015
Upper	HR1	Haean	Forest stream	38°15'N, 128°7'E	299	1083 (727)	632	595	4.9 (2.3)	1.2	13.3 (3.9)	10.1
	HR2	Mandae	Agricultural stream	38°16'N, 128°9'E	292	1415 (459)	1498	530	529.0 (595.1)	287.8	36.4 (6.3)	31.4
	HR3	Inbuk River	Tributary to Soyang	38°6'N, 128°11E	255		606	163		996.3		11.8
	HR4	Soyang River	Inflow to reservoir	38°0'N, 128°6'E	234	960 (234)	1541	654	283.5 (306.8)	104.1	12.0 (4.0)	9.6
Middle	HR5	Soyang Dam	Reservoir	37°56'N, 127°49'E	189		98	430		59.0		14.2
	HR6	Eoam Dam	Reservoir	37°52'N, 127°41'E	172		246	128		693.4		212.2
	HR7	Cheongpyeong	Reservoir outflow	37°43'N, 127°24'E	122		761	550		738.0		36.4
	HR8	North Han	N. Han outlet	37°36'N, 127°20'E	108	682 (485)	56	677	263.5 (159.7)	378.3	17.1 (5.5)	23.4
	HR9	South Han	S. Han outlet	37°31'N, 127°22'E	105		73	173		591.7		18.8
	HR10	Paldang Dam	Reservoir	37°30'N, 127°18'E	97		51	171		747.8		16.0
	HR11	Amsa	Lower Han River	37°33'N, 127°7'E	76	541 (696)	224	257	498.0 (230.6)	595.5	21.7 (5.9)	20.8
Lower	HR12	Joongnang R	Urban tributary	37°33'N, 127°2'E	66	8267 (1939)	7734	9369	2326.6 (1918.5)	4112.4	429.8 (474.7)	1396.1
	HR13	Jamwon	Lower Han River	37°31'N, 127°1'E	63		3179	1653		2552.3		140.2
	HR14	Bamseom	Lower Han River	37°32'N, 126°55'E	53	2331 (1075)	3344	1463	1224.0 (756.9)	2033.8	74.3 (55.0)	173.7
	HR15	Jeonryuri	Estuary	37°41'N, 126°39'E	23		3544	2379		111.5		88.1

The numbers in parentheses indicate the standard deviation.
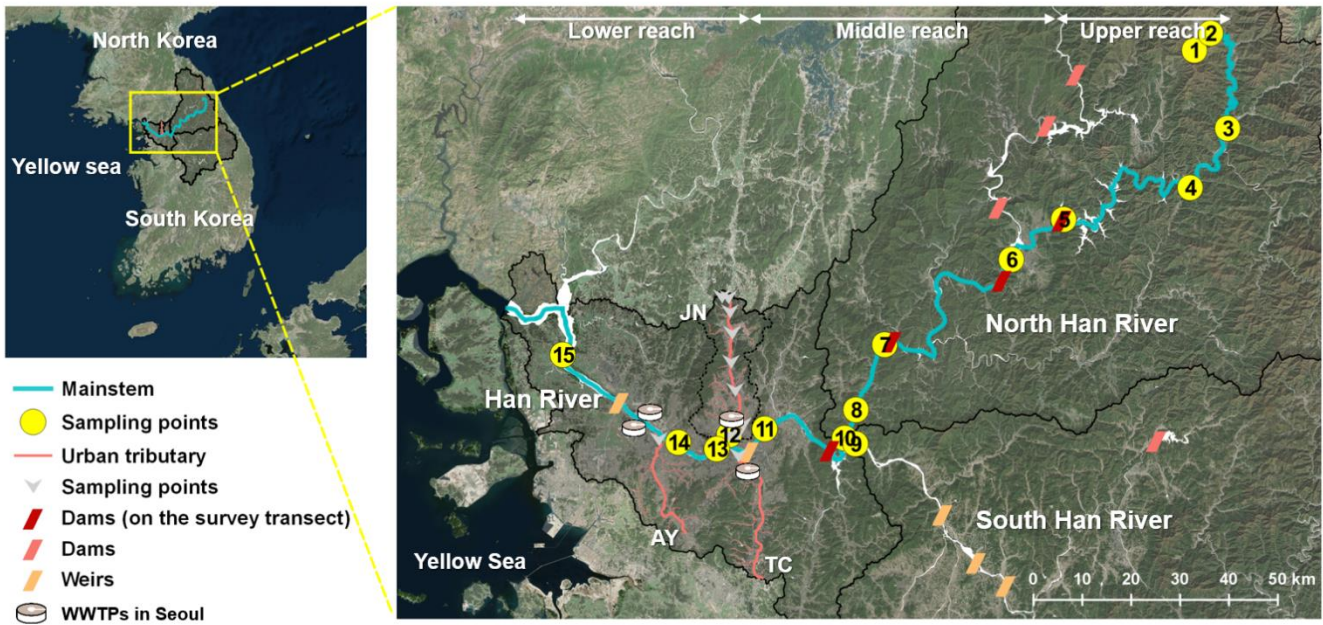
Figure 1. Study map showing sampling sites along the mainstem and three urban tributaries (JN, TC, and AY) in the Han River basin, South Korea.
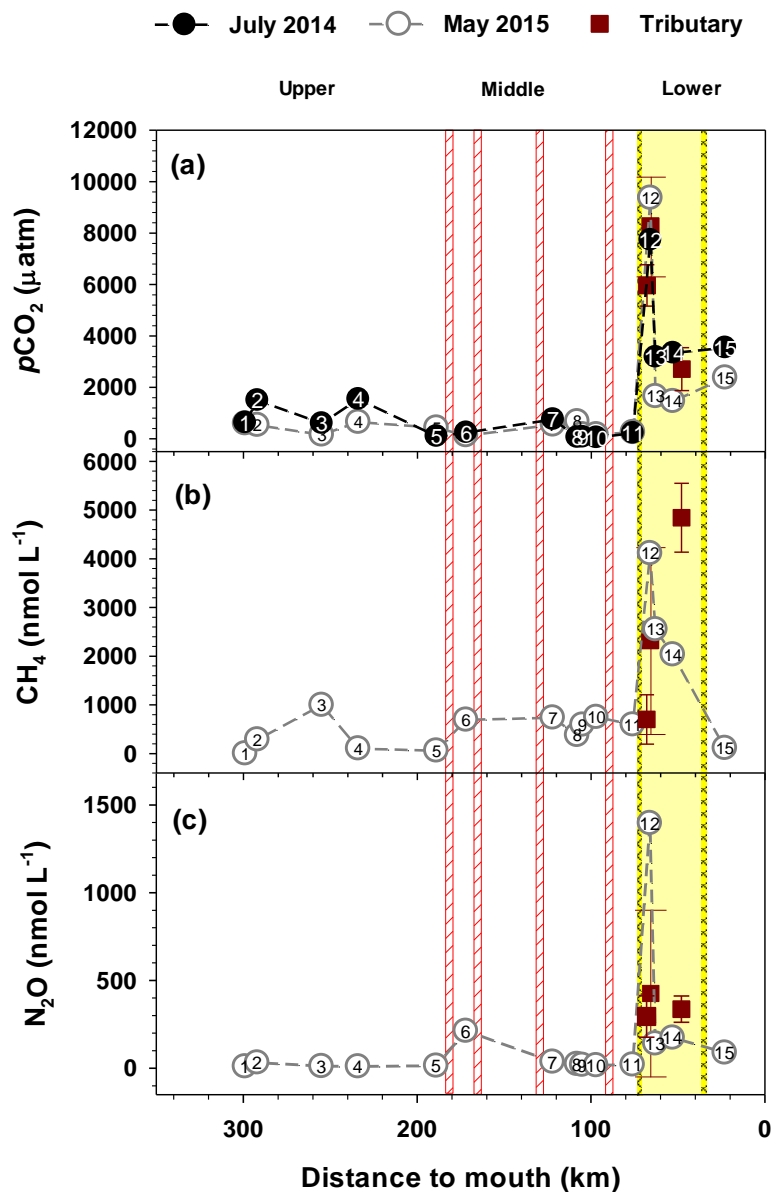
Figure 2. Spatial variations in pCO$_2$ (a), CH$_4$ (b), and N$_2$O (c) measured at 15 sites and 3 urban tributaries along the Han River. pCO$_2$ was measured in two basin-wide surveys – July 2014 and May 2015 (May 2015 data are modified from Yoon et al., 2017), but CH$_4$ and N$_2$O were measured only in May 2015. Additional measurements at the urban tributary JN (HR12; n = 13) and two other tributaries, TC (n = 4) and AN (n = 2) are indicated by brown squares with standard deviations. Dashed horizontal lines denote pCO$_2$ (435 µatm) and concentrations of dissolved CH$_4$ (3.3 nmol) and N$_2$O (6.52 nmol) equivalent to atmospheric equilibria. Four vertical lines along the middle reach indicate the location of dams. The shaded area sandwiched by two thin lines demarcate the lower reach flanked by two submerged weirs.
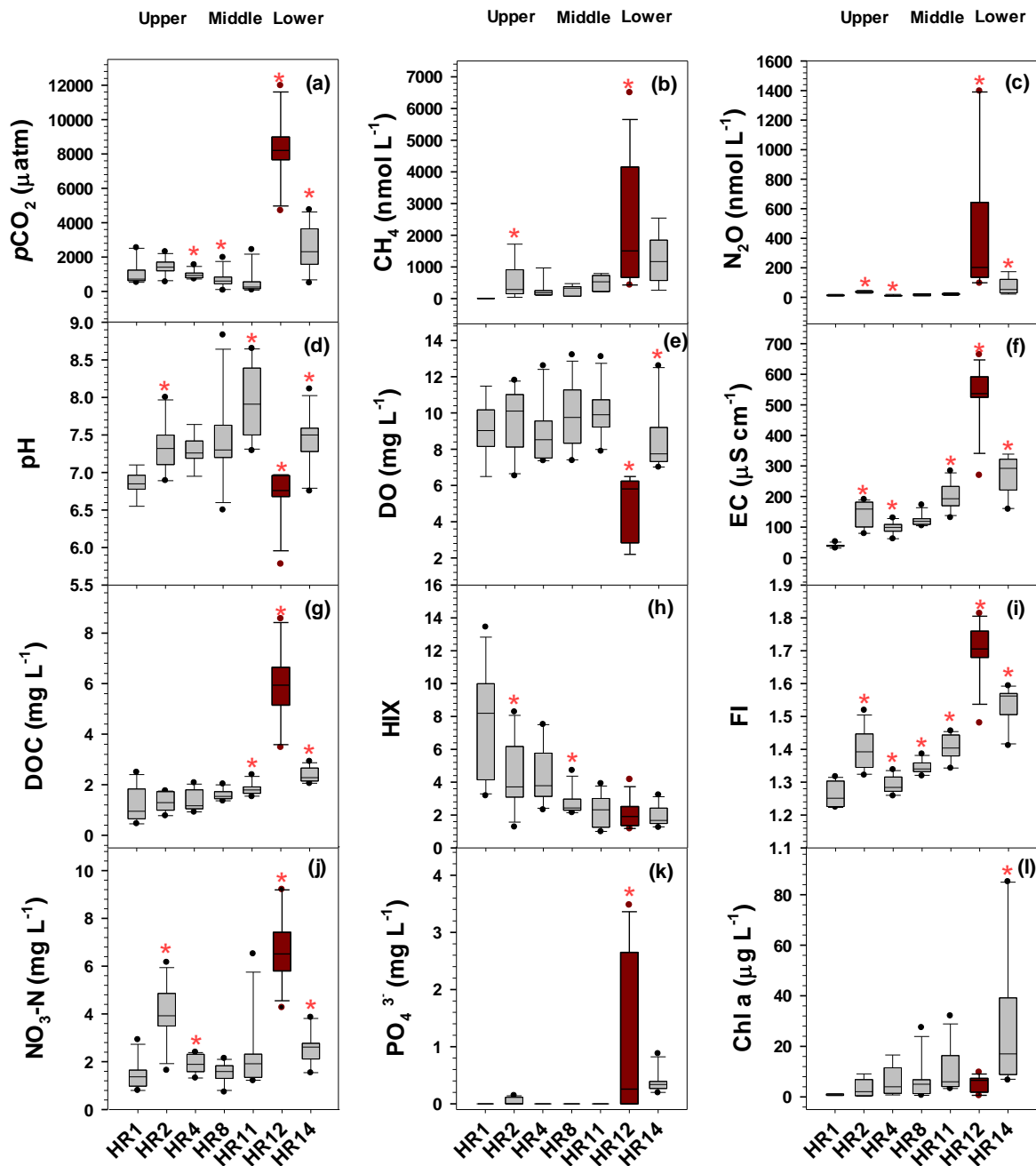
Figure 3. Box plots showing spatial variations in three GHGs (a–c), in situ measurements (d–f), DOC and optical characteristics (g–i), and concentrations of NO_3^-–N (j), PO_4^{3-} (k), and Chl a (l) measured at 6 monthly monitoring sites (July 2014–July 2015) and an urban tributary outlet (HR12; May 2015–December 2017). A significant downstream change between two successive sites is indicated by an asterisks placed on top of the downstream site (P < 0.05; Mann-Whitney test).
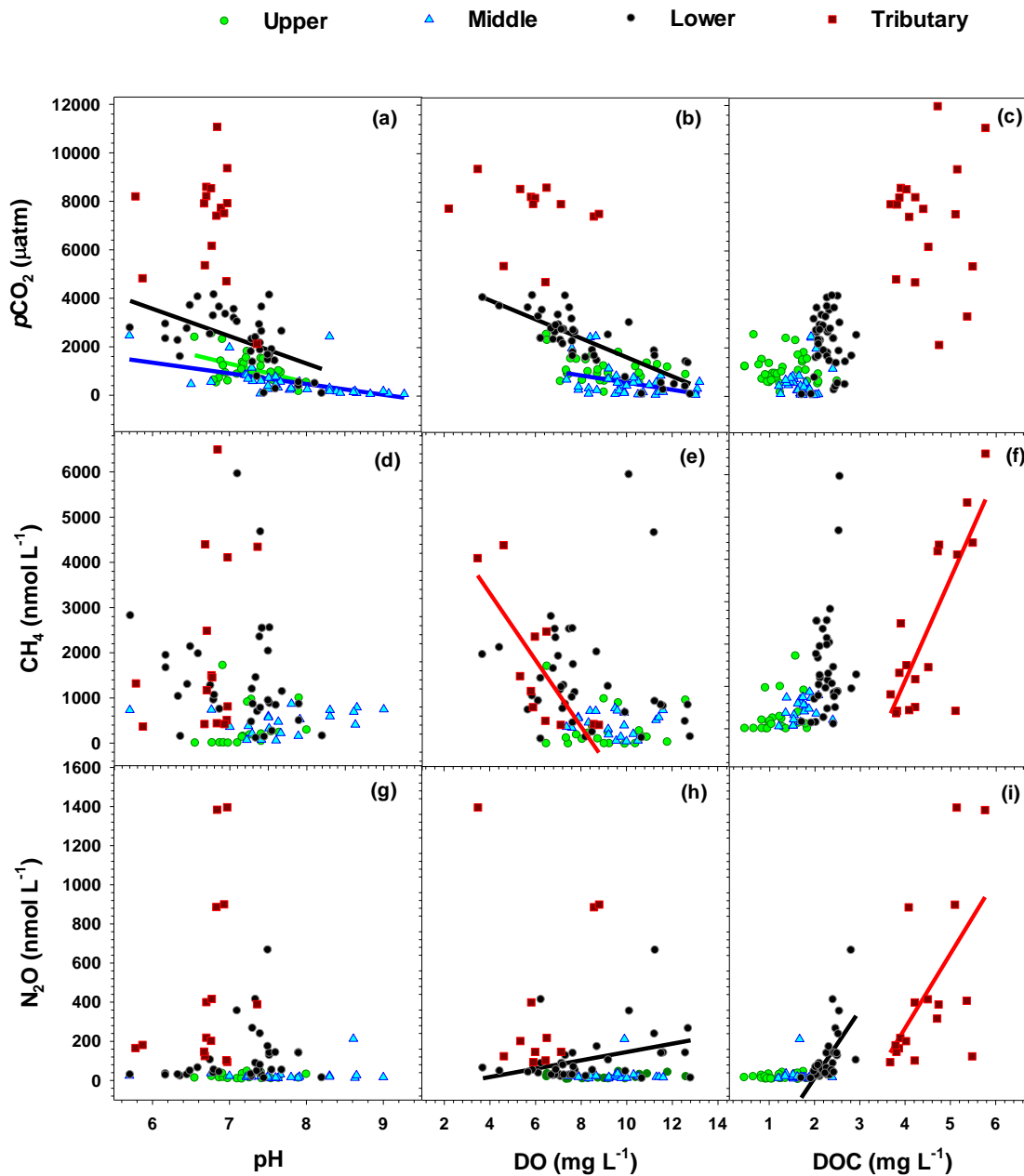
Figure 4. Relationships between water quality (pH, DO, and DOC) and dissolved concentrations of three GHGs (pCO_2, CH_4, and N_2O) measured in the Han River basin. Regression analysis was conducted with data clustered for each of the upper, middle, and lower reaches, and three urban tributaries (TC, JN, and AY). Only significant ($P < 0.05$) relationships are indicated by the regression line through the plot.
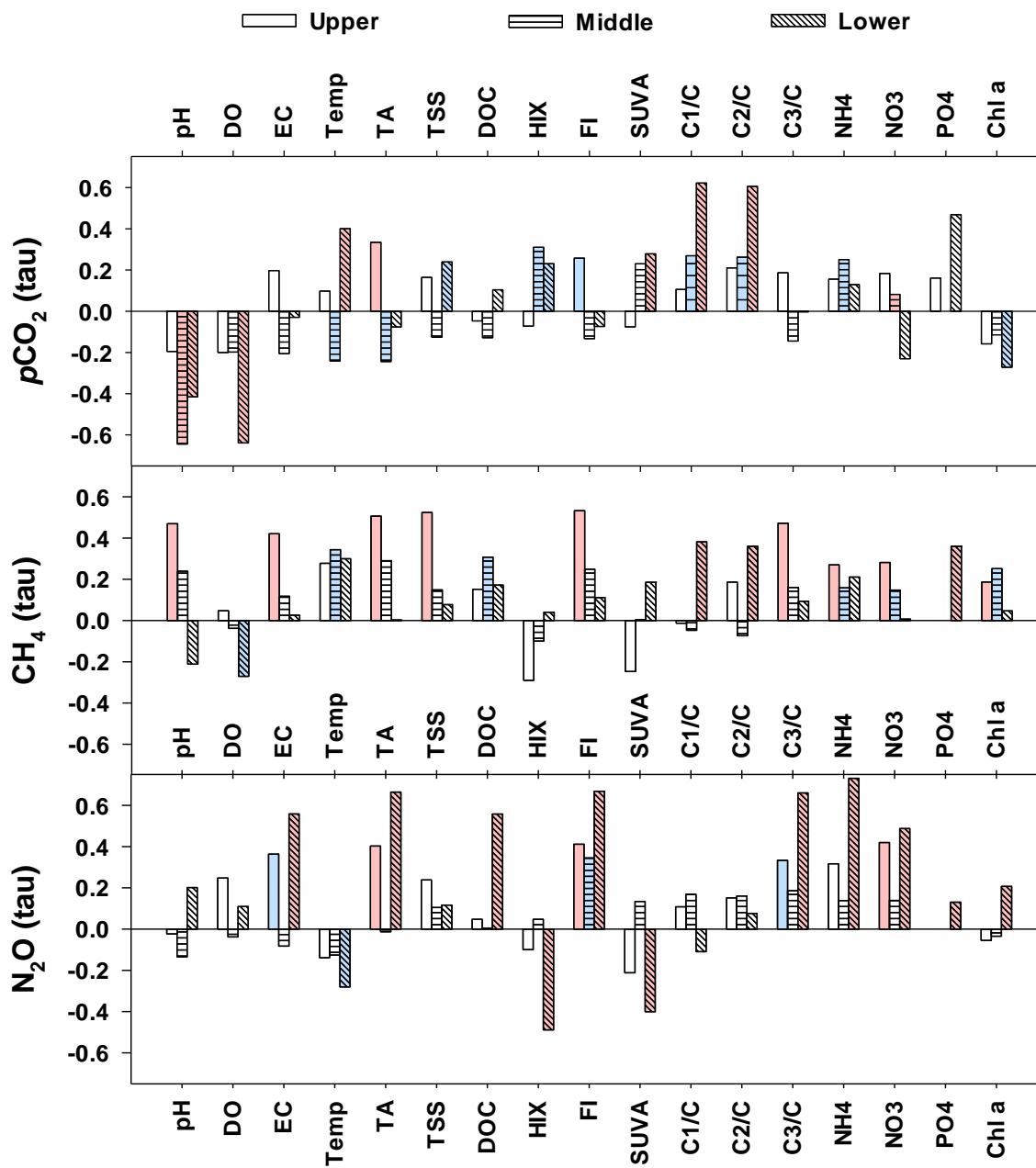
Figure 5. Kendall rank correlations (tau) between GHGs and water quality components measured in the upper, middle and lower reaches of the Han River. Significant correlations at P < 0.05 and P < 0.01 are indicated by blue and red, respectively.
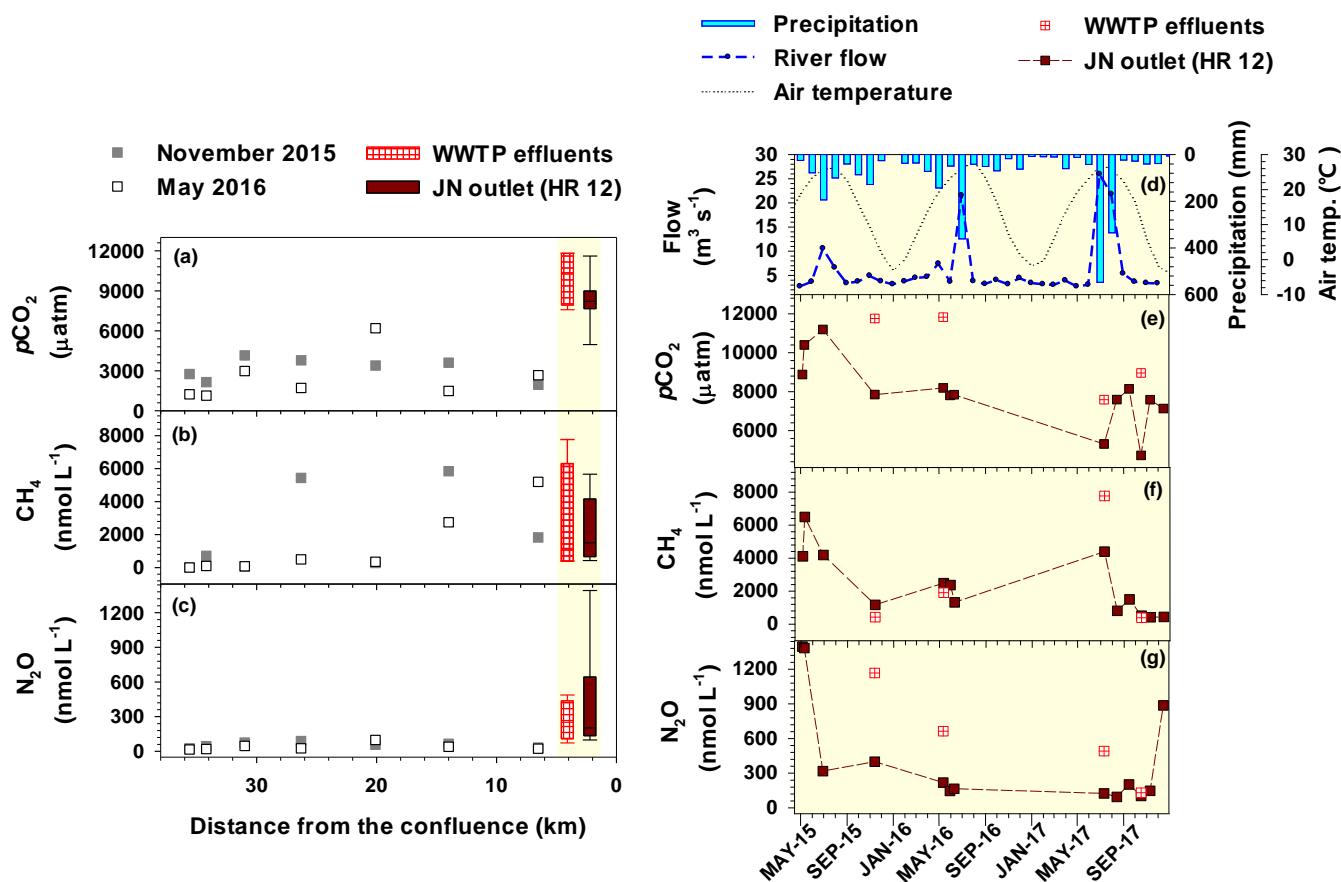
Figure 6. Longitudinal variations in pCO_2 (a; data reported in Yoon et al., 2017), CH_4 (b), and N_2O (c) along the urban tributary (Joongnang River: JN) surveyed in November 2015 and May 2016 and temporal variations in hydroclimatic conditions (d; monthly precipitation and mean temperature and flow), pCO_2 (e), CH_4 (f), and N_2O (g) monitored at the JN outlet (HR12) and WWTP effluents from May 2015 to December 2017. Box plots shown on the left panel summarize the time series data obtained from the WWTP effluents and tributary outlet, as displayed on the right panel. Weather data were obtained from an automatic weather station adjacent to HR12, while flow was measured at a bridge upstream of HR12.
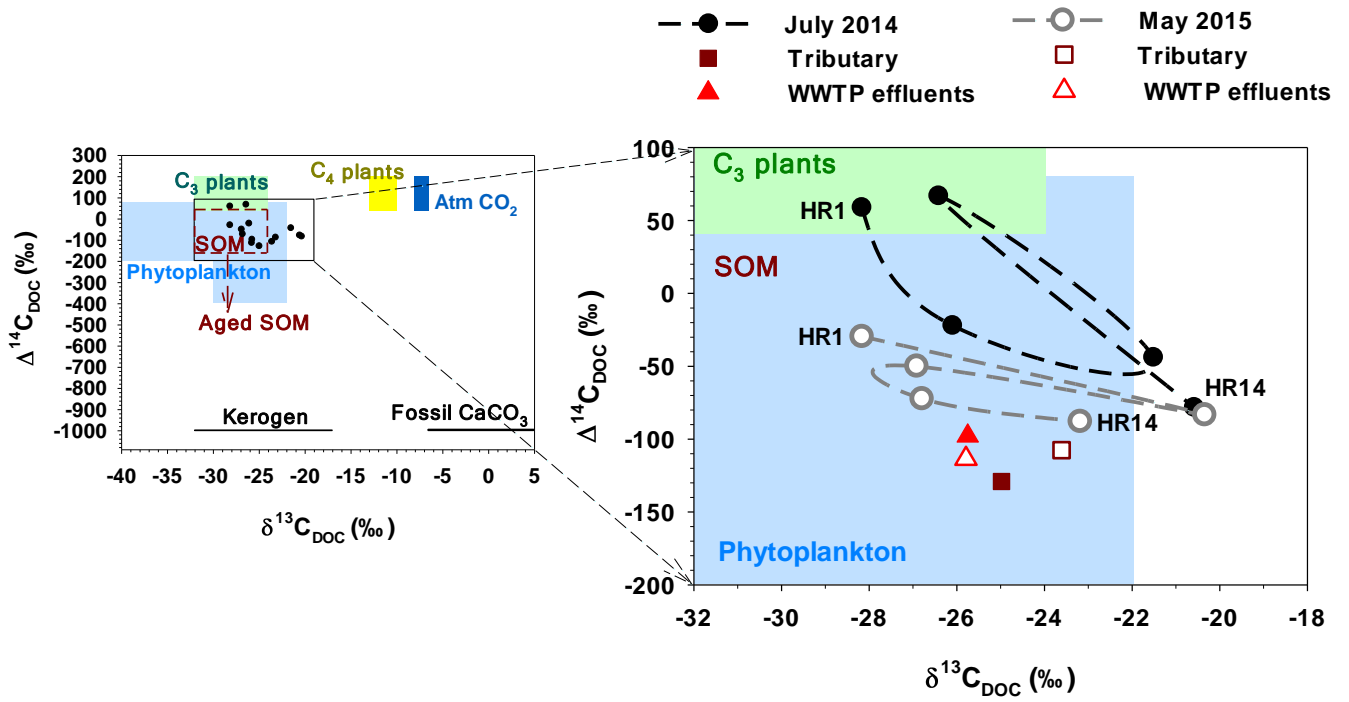
Figure 7. δ^{13}C and Δ^{14}C in DOM sampled at five Han River mainstem sites, an urban tributary, and a WWTP discharge. Mainstem (HR1, HR4, HR8, HR11, and HR14) and tributary (HR12) samples were collected in July 2014 and May 2015, whereas two WWTP effluent samples were obtained in June 2014 and November 2015. Reference values for DOM sources presented on the left plot are from Marwick et al. (2015) and references therein.
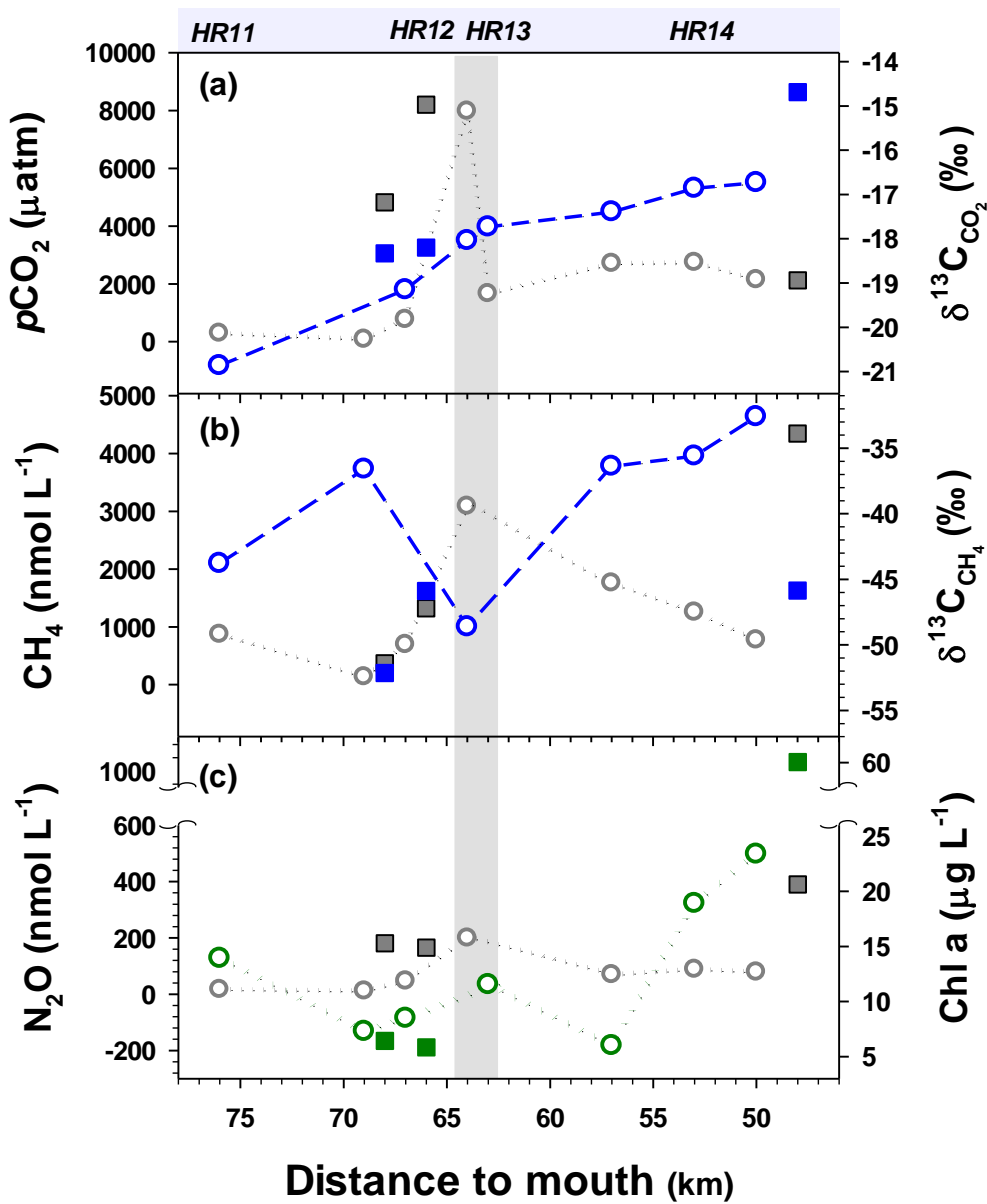
Figure 8. Spatial variations in pCO$_2$ and δ^{13}C$_{CO2}$ (a), CH$_4$ concentrations and δ^{13}C$_{CH4}$ (b), and N$_2$O and Chl a concentrations (c) measured at 8 mainstem sites and 3 urban tributary outlets during a cruise expedition (June 2016) along the lower reach of the Han River. The shaded area indicates the mainstem section receiving the inflow from the urban tributary JN (HR12). Data of pCO$_2$ and δ^{13}C$_{CO2}$ were modified from Yoon et al. (2017)